bioRxiv preprint doi: https://doi.org/10.1101/2021.09.14.460218; this version posted September 14, 2021. The copyright holder for this preprint (which was not certified by peer review) is the author/funder, who has granted bioRxiv a license to display the preprint in perpetuity. It is made available under aCC-BY 4.0 International license.

Direct capsid labeling of infectious HIV-1 by genetic code expansion allows detection of largely complete nuclear capsids and suggests nuclear entry of HIV-1 complexes via common routes

Sandra Schifferdecker[1], Vojtech Zila[1], Thorsten G. Müller[1], Volkan Sakin[1], Maria Anders-Össwein[1], Vibor Laketa[1,2], Hans-Georg Kräusslich[1,2], Barbara Müller[1*]

[1] Department of Infectious Diseases, Virology, University Hospital Heidelberg, Heidelberg, Germany

[2] German Center for Infection Research, partner site Heidelberg, Germany

*To whom correspondence should be addressed: Barbara.mueller@med.uni-heidelberg.de

Keywords: HIV-1, capsid, click labeling, amber suppression, genetic code expansion, primary CD4$^+$ T cells, electron microscopy, correlative microscopy, STED, super-resolution microscopy

bioRxiv preprint doi: https://doi.org/10.1101/2021.09.14.460218; this version posted September 14, 2021. The copyright holder for this preprint (which was not certified by peer review) is the author/funder, who has granted bioRxiv a license to display the preprint in perpetuity. It is made available under aCC-BY 4.0 International license.

Abstract

The cone-shaped mature HIV-1 capsid is the main orchestrator of early viral replication. After cytosolic entry, it transports the viral replication complex along microtubules towards the nucleus. Capsid uncoating from the viral genome apparently occurs beyond the nuclear pore. Observation of post-entry events *via* microscopic detection of HIV-1 capsid protein (CA) is challenging, since epitope shielding limits immunodetection, and the genetic fragility of CA hampers other labeling approaches. Here, we present a minimally invasive strategy based on genetic code expansion and click chemistry that allows for site-directed fluorescent labeling of HIV-1 CA, while retaining virus morphology and infectivity. Thereby, we could directly visualize virions and subviral complexes using advanced microscopy, including nanoscopy and correlative imaging. Quantification of signal intensities of subviral complexes showed that the amount of CA associated with nuclear complexes in HeLa-derived cells and primary T cells is consistent with a complete capsid and revealed that treatment with the small molecule inhibitor PF74 did not result in capsid dissociation from nuclear complexes. Cone-shaped objects detected in the nucleus by electron tomography were clearly identified as capsid-derived structures by correlative microscopy. High-resolution imaging revealed dose-dependent clustering of nuclear capsids, suggesting that incoming particles may follow common entry routes.

bioRxiv preprint doi: https://doi.org/10.1101/2021.09.14.460218; this version posted September 14, 2021. The copyright holder for this preprint (which was not certified by peer review) is the author/funder, who has granted bioRxiv a license to display the preprint in perpetuity. It is made available under aCC-BY 4.0 International license.

Introduction

The cone-shaped capsid that encases the viral RNA genome and replication proteins is a characteristic feature of infectious human immunodeficiency virus type 1 (HIV-1) particles. Data obtained by many research groups over the past decade have revised our understanding of the role of the mature capsid in HIV-1 replication, placing this structure at the center stage of post-entry replication steps (reviewed in Campbell and Hope, 2015; Novikova *et al.*, 2019; Engelman, 2021; Guedán *et al.*, 2021; Toccafondi, Lener and Negroni, 2021). Upon fusion of the virion envelope with the cell membrane, the capsid, which consists of ~1,200-1,500 monomers of the capsid protein CA (Briggs et al. 2003), is released into the cytosol. It then usurps host cell factors to traffic towards the nucleus. Reverse transcription of the viral RNA into dsDNA is initiated during passage of the subviral structure through the cytosol. Following import into the nucleus, the viral dsDNA is covalently integrated into the host cell genome by the viral integrase. Prior to integration, the surrounding capsid shell needs to expose the dsDNA in a process termed uncoating. However, the precise mechanisms, location, and timing of capsid uncoating are still under investigation.

Initially, the HIV-1 capsid was presumed to rapidly dissociate upon cell entry, based on its instability observed in early biochemical analyses (Miller, Farnet, and Bushman 1997; Bukrinsky et al. 1993; Fassati and Goff 2001). Rapid or gradual disassembly in the cytosol was also supported by several studies applying fluorescence imaging to analyze subviral complexes in infected cells (Hulme, Perez and Hope, 2011; Xu *et al.*, 2013; Cosnefroy, Murray and Bishop, 2016; Mamede *et al.*, 2017). However, the finding that CA, or even the capsid lattice, directly interacts with various host factors involved in post-entry replication steps - including not only cytosolic proteins but also nucleoporins and even the nuclear protein CPSF6 (e.g., Schaller *et al.*, 2011; Price *et al.*, 2012; Di Nunzio *et al.*, 2013; Matreyek *et al.*, 2013; Bhattacharya *et al.*, 2014; Lelek *et al.*, 2015; Rebensburg *et al.*, 2021) - implicated involvement of at least a partial lattice structure in later stages of post-entry replication. Furthermore, increasing evidence from imaging-based analyses argued for capsid uncoating at the nuclear pore (Arhel et al. 2007; Burdick et al. 2017; Rodriguez, Lester, and Dougherty 2007; Francis et al. 2016; Francis and Melikyan 2018; Francis, Marin, Prellberg, et al. 2020; Rasaiyaah et al. 2013), or even for the passage of capsids or capsid-related structures through nuclear pores (Zila et al. 2021; Selyutina et al. 2020; T. G. Müller et al. 2021; Dharan et al. 2020; Burdick et al. 2020). The recent detection of cone-shaped objects

bioRxiv preprint doi: https://doi.org/10.1101/2021.09.14.460218; this version posted September 14, 2021. The copyright holder for this preprint (which was not certified by peer review) is the author/funder, who has granted bioRxiv a license to display the preprint in perpetuity. It is made available under aCC-BY 4.0 International license.

in the nuclear pore channel and inside the nucleus by correlative light and electron microscopy (CLEM), and intranuclear separation of CA or IN from reverse transcribed dsDNA also support the model that the nucleus is the site of HIV-1 uncoating (Li et al. 2021; Burdick et al. 2020; Zila et al. 2021; T. G. Müller et al. 2021).

One explanation for apparent discrepancies between different studies are the methods that have been used for CA detection in fluorescence microscopy. Since the modification of CA by genetic labeling strategies proved to be challenging, most studies applied immunofluorescence (IF) staining or other indirect labeling approaches (Francis et al. 2016; Francis and Melikyan 2018; Francis, Marin, Prellberg, et al. 2020; Márquez et al. 2018; Mamede et al. 2017; Hulme, Perez, and Hope 2011; Hulme and Hope 2014). A limitation of IF is that staining efficiency may vary substantially depending on the antibody and detection conditions used, as well as on differential exposure or shielding of epitopes due to conformational changes or different intracellular environments. We could indeed show previously that immunostaining efficiency of CA in the nucleus of host cells strongly depends on cell type and experimental conditions (T. G. Müller et al. 2021). Furthermore, IF is incompatible with live cell analyses. Infectious HIV-1 derivatives carrying fluorescent CA would resolve these limitations and allow the direct observation of entering capsids with quantitative analyses.

However, viral capsid proteins are intrinsically challenging targets for genetic labeling. They are generally small proteins that need to self-assemble into ordered multimeric lattices. The resulting assemblies must be stable during virus formation and transmission to a new target cell, but also ready to disassemble in the newly infected cell, requiring structural flexibility of the protomers. Beyond protein-protein interactions involved in capsid assembly itself, capsid proteins generally undergo crucial interactions with other components of the virion, e.g., the viral genome. Finally, the capsid surface represents an essential contact interface between virus and host cell in the early phase of infection, mediating cell entry in the case of non-enveloped viruses, or interacting with critical host cell dependency or restriction factors in the case of enveloped viruses. Consequently, a large proportion of the surface exposed amino acids of a viral capsid protein is involved in intermolecular contacts that are crucial for virus replication, which renders these proteins highly susceptible to genetic modification. Fusion of a capsid protein to a relatively large genetic label, e.g., green

bioRxiv preprint doi: https://doi.org/10.1101/2021.09.14.460218; this version posted September 14, 2021. The copyright holder for this preprint (which was not certified by peer review) is the author/funder, who has granted bioRxiv a license to display the preprint in perpetuity. It is made available under aCC-BY 4.0 International license.

fluorescent protein (GFP) or other fluorescent proteins, is thus generally prone to severely affect virus infectivity.

These considerations also apply to HIV-1 CA. The protein is encoded as a subdomain of the structural polyprotein Gag, from which it is released by the viral protease (PR) concomitant with virus budding to allow for formation of the mature capsid. With a molecular mass of ~24 kDa, mature CA is of a similar size as GFP. Hexa- and pentamers of CA are the core structural elements of the immature Gag polyprotein shell forming the nascent virus bud in HIV-1 producing cells, as well as of the mature capsid lattice. CA pentamers, immature and mature hexamers employ different protein-protein interfaces; together, these interfaces involve most of the exposed surface of the CA monomer (Mattei et al. 2016; Zhao et al. 2013; Grime and Voth 2012; Ganser-Pornillos, Cheng, and Yeager 2007; Pornillos, Ganser-Pornillos, and Yeager 2011). Accordingly, scanning mutagenesis analyses found HIV-1 CA to be highly genetically fragile (von Schwedler *et al.*, 2003; Fassati, 2012; Rihn *et al.*, 2013), with up to 89% of single amino acid exchanges tested abolishing or severely affecting virus replication (Rihn et al. 2013). It is thus not surprising that the introduction of genetically encoded labels - GFP or even a small peptide tag - at various positions within HIV-1 CA have resulted in loss or severe reduction of infectivity (Pereira et al. 2011; Campbell et al. 2008; Ma et al. 2016; Burdick et al. 2020; Zurnic Bönisch et al. 2020). Complementation with wild-type (wt) virus, from at least equimolar amounts of wt CA to a substantial molar excess, was essential to restore infectivity (Campbell et al. 2008; Burdick et al. 2020; Zurnic Bönisch et al. 2020). While the use of wt complemented particles can be sufficient for fluorescent labeling, it is unclear whether the modified CA molecules are an integral part of the mature CA lattice; only ~ 50% of CA molecules present inside the virion are eventually used to form the mature capsid (J. A G Briggs et al. 2004; Lanman et al. 2004), and incorporated fusion proteins may be preferentially excluded from the mature lattice.

We therefore established and applied a minimal invasive labeling strategy for HIV-1 CA based on genetic code expansion and click labeling. This method involves the exchange of a selected amino acid residue in the protein of interest with a non-canonical amino acid (ncAA) carrying a highly reactive bio-orthogonal functional group by a process termed amber suppression (Figure 1a); this residue is subsequently covalently coupled to a fluorophore functionalized with a cognate reaction partner (Figure 1a; Lang and Chin, 2014; Nikić and Lemke, 2015; Kelemen, Erickson and

bioRxiv preprint doi: https://doi.org/10.1101/2021.09.14.460218; this version posted September 14, 2021. The copyright holder for this preprint (which was not certified by peer review) is the author/funder, who has granted bioRxiv a license to display the preprint in perpetuity. It is made available under aCC-BY 4.0 International license.

Chatterjee, 2018; Müller, Sakin and Müller, 2019; Krauskopf and Lang, 2020; de la Torre and Chin, 2021). Using this approach, we generated a CA-labeled HIV-1 derivative that largely retained infectivity; in contrast to previous approaches for direct CA labeling, our minimally modified derivative did not require complementation with wt virus. Direct labeling with a bright and photostable chemical dye allows the application of various imaging methods, i.e., live-cell imaging, super-resolution nanoscopy, or CLEM. The virus variant click labeled with a bright and photostable chemical dye thus enabled us to directly assess the amount of CA associated with entering subviral complexes outside and within the nucleus of infected HeLa-derived cells and primary $CD4^+$ T-cells, to visualize CA containing structures in the nucleus by nanoscopy and correlative microscopy and to study the effect of the CA-binding drug PF74 on the nuclear complexes.

Results

Generation of an HIV-1 variant carrying a bio-orthogonal amino acid within CA

To allow for minimally invasive labeling of HIV-1 CA by genetic code expansion (GCE; Figure 1a), we introduced an amber stop codon at a position of interest into the CA coding sequence within the *gag* open reading frame of the proviral plasmid pNLC4-3 (Bohne and Kräusslich 2004). In order to avoid GCE modification of the viral protein R (Vpr), which is incorporated into the virion in high amounts (B. Müller et al. 2000), we first exchanged the amber stop codon of *vpr* to an opal codon (TGA), resulting in plasmid pNLC4-3*. Albeit this mutation did not alter the coding sequence of viral proteins or virion infectivity, the corresponding virus was termed HIV-1* to indicate this modification. Since neither the efficiency of amber suppression in a given sequence context in eukaryotic cells, nor the effect of ncAA incorporation on viral functionality can be predicted with certainty, we tested a panel of 19 amber mutations at sites located towards the outer surface of the capsid lattice for suppression efficiency and virus infectivity (Schifferdecker, Sakin et al., in preparation). Based on a comparison of Gag expression levels and viral infectivity upon ncAA incorporation, we selected a virus variant in which residue alanine 14 in CA was replaced by a non-canonical amino acid (HIV-1*CA14^{ncAA}) for further analyses.

bioRxiv preprint doi: https://doi.org/10.1101/2021.09.14.460218; this version posted September 14, 2021. The copyright holder for this preprint (which was not certified by peer review) is the author/funder, who has granted bioRxiv a license to display the preprint in perpetuity. It is made available under aCC-BY 4.0 International license.

For virus preparation, HEK293T cells were co-transfected with the respective mutant proviral plasmid and pNESPlyRS-eRF1dn-tRNA. The latter plasmid encodes for a complete amber suppression system, consisting of modified tRNA, a cognate genetically engineered pyrrolysine aminoacyl-tRNA synthetase (Nikić et al. 2016), and a dominant-negative version of the eukaryotic release factor eRF1 that improves amber suppression efficiency in eukaryotic cells (Schmied et al. 2014). To produce functionalized virus particles, cells were grown in the presence of the small ncAA cyclopropene lysine (CpK). While truncation of Gag at position 14 of CA would prevent virus formation, incorporation of CpK by amber suppression should result in the expression of full-length Gag and thereby promote HIV-1 particle assembly. Immunoblot analysis of cell lysates indeed demonstrated the presence of full-length Gag polyprotein precursor when HIV-1*CA14^{TAG} expressing cells were grown in the presence of CpK, whereas full-length Gag was not detected when CpK was omitted from the growth medium (Figure 1 – figure supplement 1). Thin-section electron microscopy (EM) revealed late budding sites and immature- as well as mature-like virions at the plasma membrane and in the vicinity of HIV-1*CA14^{ncAA} expressing cells, that were morphologically indistinguishable from typical HIV-1 wild-type (wt) budding sites and virions (Figure 1b). We concluded that Gag expression of HIV-1*CA14^{TAG} is ncAA dependent and the modified CA domain is competent for immature and mature lattice assembly.

Characterization of click labeled HIV-1 virions

We next prepared virus particles from the supernatant of HIV-1*CA14^{ncAA} producing cells and subjected them to click labeling using the membrane-permeable dye silicon rhodamine tetrazine (SiR-Tet; (Lukinavičius *et al.*, 2013)), generating HIV-1*CA14^{SiR}. As a control, HIV-1* wt particles were prepared under amber suppression conditions and stained in parallel. Consistent with the detection of viral assembly sites and particles in electron micrographs (Figure 1b), virus was recovered from the tissue culture supernatant of HIV-1*CA14^{ncAA} expressing cells. Particle yields were somewhat reduced compared to the HIV-1* wt control, in line with the fact that amber suppression is usually incomplete in eukaryotic cells (optimal ncAA incorporation efficiencies in the range of ~25-50 %; (Rodriguez, Lester, and Dougherty 2007; Schmied et al. 2014; Sakin et al. 2017)). On average, we obtained 5-10-fold lower yields for HIV-1*CA14^{SiR}

bioRxiv preprint doi: https://doi.org/10.1101/2021.09.14.460218; this version posted September 14, 2021. The copyright holder for this preprint (which was not certified by peer review) is the author/funder, who has granted bioRxiv a license to display the preprint in perpetuity. It is made available under aCC-BY 4.0 International license.

compared to HIV-1* (Figure 1c, d). Consistent with the observation of morphologically mature particles by EM, click labeled particles displayed regular Gag and GagPol processing products (Figure 1e), with clear bands for mature RT heterodimer (p51, p66) and mature CA (p24). In-gel fluorescence revealed a distinct SiR labeled band corresponding to a mass of approximately 24 kDa for HIV-1*CA14^{SiR}, but not for HIV-1* control particles (Figure 1f). Taken together, these findings indicate specific GCE-dependent labeling of CA *via* amber suppression at position 14 of HIV-1 CA.

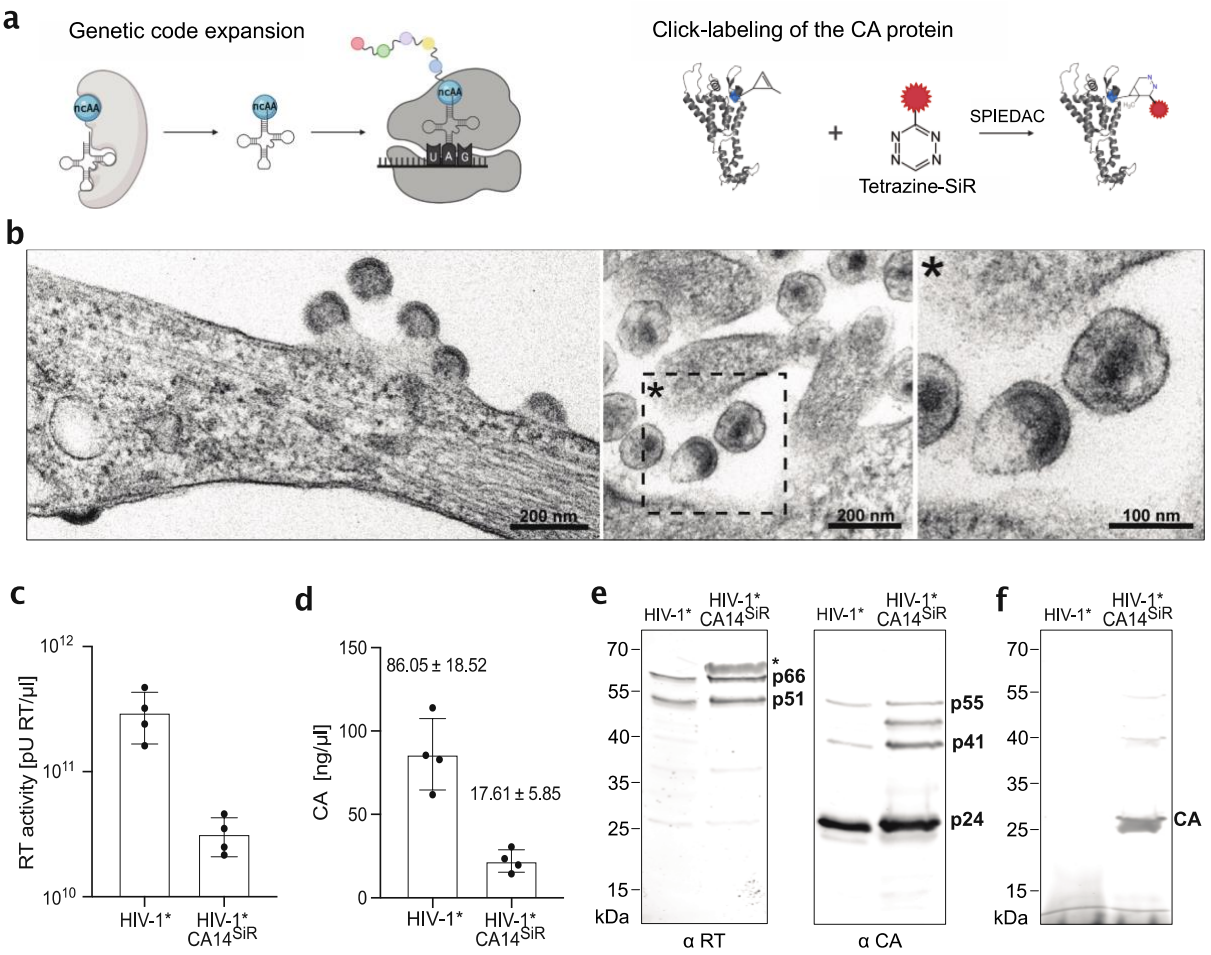

Figure 1. Production and characterization of click labeled HIV-1 (HIV-1*CA14^{SiR}). **(a)** Experimental scheme for GCE and click-labeling. The system used here requires the introduction of an amber stop codon (UAG) at a specific site into the coding sequence of the protein of interest. A genetically engineered bio-orthogonal tRNA / aminoacyl-tRNA synthetase pair mediates incorporation of a non-canonical amino acid (ncAA) at the chosen position. In a second step, a highly reactive group of the ncAA is covalently linked to a fluorophore carrying a cognate reactive group (e.g., a tetrazine group reacting with a cyclopropane group at the ncAA *via* strain-promoted inverse

bioRxiv preprint doi: https://doi.org/10.1101/2021.09.14.460218; this version posted September 14, 2021. The copyright holder for this preprint (which was not certified by peer review) is the author/funder, who has granted bioRxiv a license to display the preprint in perpetuity. It is made available under aCC-BY 4.0 International license.

electron-demand Diels-Alder cycloaddition (SPIEDAC)). Image created with BioRender.com **(b)** Morphology of HIV-1*CA14^{ncAA} assembly sites and particles. HEK293T cells were co-transfected with pNLC4-3*CA14^{TAG} and pNESPlyRS-eRF1dn-tRNA and grown in the presence of 550 µM CpK. At 44 h p.t., cells were fixed, embedded, and analyzed by thin-section EM as described in materials and methods. **(c,d)** Virus production. Click labeled particles were prepared from the supernatant of HEK293T cells co-transfected with either pNLC4-3* or pNLC4-3*CA14^{TAG} and pNESPlyRS-eRF1dn-tRNA. Cells were grown in the presence of 500 µM CpK as described in materials and methods. Particle yield in the final preparations was determined via quantitation of RT activity (SG-PERT assay;(Pizzato et al. 2009)) **(c)** and by determination of CA amounts using quantitative immunoblot as described in materials and methods **(d)**. The graphs show mean values and SD from four independent experiments. **(e)** Immunoblot analysis of virus preparations. Particle lysates were separated by SDS-PAGE, and proteins were transferred to nitrocellulose membranes by semi-dry blotting. Viral proteins were detected using polyclonal antisera raised against recombinant HIV-1 RT or CA. Bound antibodies were detected by quantitative immunofluorescence with a Li-COR CLx infrared scanner, using secondary antibodies and protocols according to the manufacturer's instructions. An asterisk indicates non-specific reactivity with bovine serum albumin carried over from the medium **(f)** In-gel fluorescence. Particle lysates prepared as in (e) were separated by SDS-PAGE, and the acrylamide gel was scanned using a Li-COR CLx infrared scanner set at an emission wavelength of 700 nm.

Fluorescence labeling and infectivity of click labeled virions

To test specificity and efficiency of SiR staining, labeled particles adhered to a glass chamber slide were fixed, permeabilized, and immunostained with antiserum raised against HIV-1 CA to validate that detected signals corresponded to virus particles. Confocal micrographs were recorded in the channels corresponding to the CA immunofluorescence (IF) stain (green) and direct CA labeling with SiR (magenta) (Figure 2a). Regions of interest (ROIs) corresponding to the position of virus particles were defined based on CA(IF) signals. Measurement of SiR fluorescence intensities in these ROIs revealed weak background staining in the case of HIV-1* (Figure 2a, left panel). In contrast, distinct SiR signals co-localizing with CA(IF) punctae were detected

bioRxiv preprint doi: https://doi.org/10.1101/2021.09.14.460218; this version posted September 14, 2021. The copyright holder for this preprint (which was not certified by peer review) is the author/funder, who has granted bioRxiv a license to display the preprint in perpetuity. It is made available under aCC-BY 4.0 International license.

for HIV-1*CA14^{SiR} (Figure 2a, right panel). Quantitative analyses of images from multiple independent experiments confirmed this visual impression (Figure 2b). Only ~8.5% of HIV-1* particles were classified as SiR positive, with fluorescence intensities only slightly above the background level (~1,000 a.u.). In contrast, >95% HIV-1*CA14^{SiR} particles displayed clear SiR staining, with a mean fluorescence intensity of ~15,000 a.u. Variation in SiR fluorescence intensities between individual particles is expected, since particle size and CA content of HIV-1 virions varies, with ~1,700-3,100 CA monomers estimated per particle (Carlson et al. 2008). Beyond that, the range of SiR signal intensities observed also indicates a range of click labeling efficiencies. Despite some variability in the preparation, the vast majority of HIV-1*CA14^{CpK} particles could be efficiently click labeled with SiR, attaining fluorescence intensities suitable for fluorescence microscopy of infected cells.

To test the effect of introducing a synthetic fluorophore at position 14 on CA functionality, the infectivity of click labeled particles was assessed by titration of labeled particles on TZM-bl cells, followed by immunostaining against the HIV-1 matrix protein (MA) to identify infected cells. As shown in Figures 2c and d, relative infectivity of HIV-1*CA14^{SiR} was only mildly reduced by an average of ~2-fold compared to HIV-1*, a substantial improvement compared to previous genetic labeling strategies (Campbell et al. 2008; Burdick et al. 2020; Zurnic Bönisch et al. 2020; Pereira et al. 2011). Thus, minimal invasive labeling by GCE allows direct labeling of HIV-1 CA without requiring complementation with wt virus.

bioRxiv preprint doi: https://doi.org/10.1101/2021.09.14.460218; this version posted September 14, 2021. The copyright holder for this preprint (which was not certified by peer review) is the author/funder, who has granted bioRxiv a license to display the preprint in perpetuity. It is made available under aCC-BY 4.0 International license.

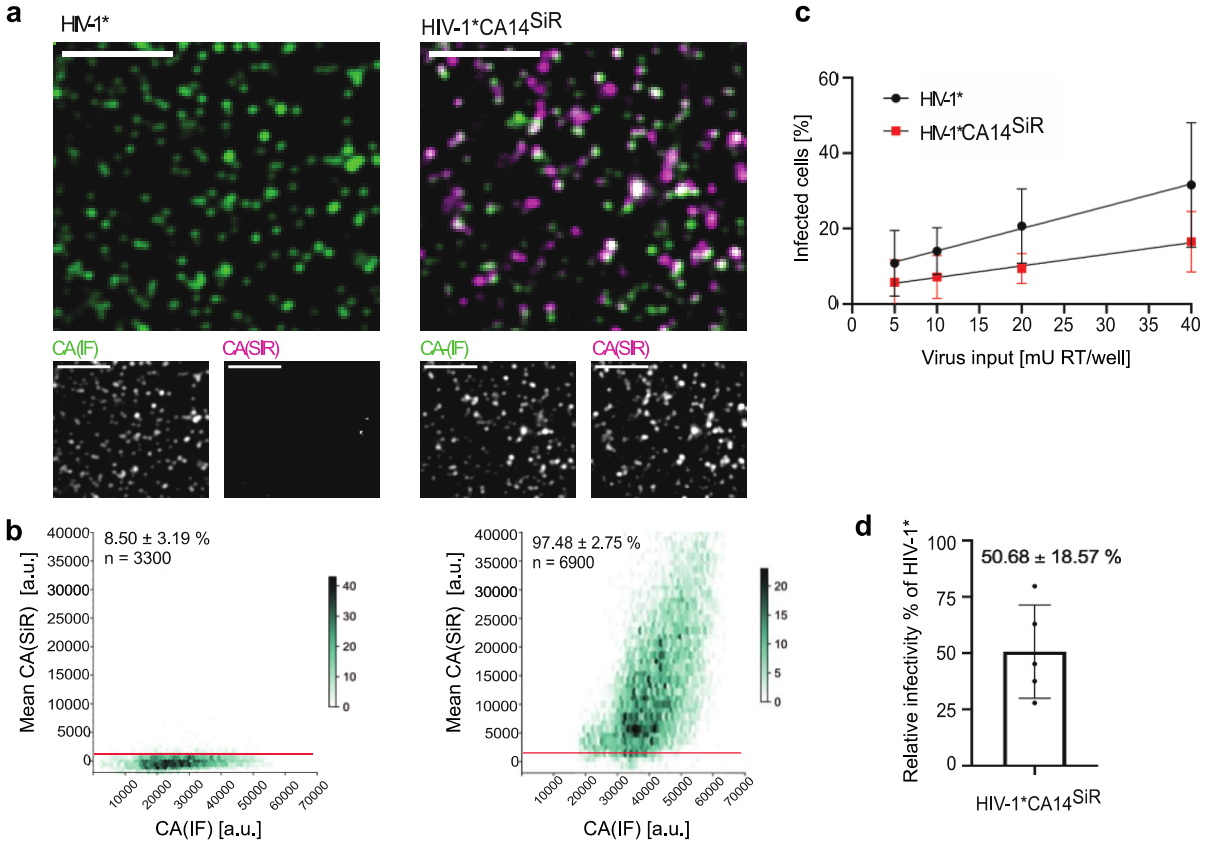

Figure 2. Characterization of CA click labeled particles. (a) Analysis of labeling efficiency. Particles harvested from the supernatant of virus producing HEK239T cells were subjected to click labeling. Particles were then immobilized on PEI coated chamber slides, fixed, and permeabilized. Particles were immunostained using antiserum raised against HIV-1 CA, and specimens were imaged by spinning disk confocal microscopy (SDCM). Scale bars 5 µm. **(b)** Hexabin plots of detected particles. Mean intensities of CA(SiR) are plotted against mean intensity CA(IF) for HIV-1* and HIV-1*CA14^{SiR}. The color intensity of the hexagons corresponds to the number of particles displaying the indicated intensity values. The graphs represent pooled data from 12 fields of view from three independent virus preparations. The red line indicates the threshold t=1,000. **(c)** Infectivity of click labeled particles. The indicated virus particles were prepared as in (a) and subjected to click labeling. Particle yield was assessed by RT activity assay (Pizzato et al. 2009), and samples were titrated on TZM-bl indicator cells seeded in 15-well ibidi µ-angiogenesis slides. 50 µM T-20 was added at 6 h p.i. to prevent second-round infection in the case of wt. Cells were fixed, permeabilized, and immunostained using a polyclonal rabbit antiserum raised against recombinant HIV-1 MA at 48 h p.i. Samples were imaged by SDCM. The percentage

bioRxiv preprint doi: https://doi.org/10.1101/2021.09.14.460218; this version posted September 14, 2021. The copyright holder for this preprint (which was not certified by peer review) is the author/funder, who has granted bioRxiv a license to display the preprint in perpetuity. It is made available under aCC-BY 4.0 International license.

of infected cells was determined using Fiji software. The graphs show mean values and SD from five independent infection experiments using five independent particle preparations (n=5,700-7,700 cells were counted per condition). Lines represent linear regression based on the mean values. **(d)** Relative infectivity of a virus preparation (% infected cells/mU RT) was determined as in (c), and the values obtained for HIV-1*CA14^{SiR} were normalized to the value obtained for HIV-1* virus in the same experiment. All cells counted in (c) were used for quantification. The graph represents the mean value and SD from five independent experiments.

Detection of click labeled HIV-1 in infected cells

Having established a suitable labeling strategy, we used labeled particles to infect target cells. Initial experiments were performed in HeLa TZM-bl cells (Wei et al. 2002), a widely used model cell line in HIV-1 research. Cells infected with HIV-1*CA14^{SiR} at an MOI~0.8 were fixed at 18 h post infection (h p.i.). Immunostaining with antiserum against CA was performed under conditions that allow for immunodetection of cytosolic and nuclear complexes (T. G. Müller et al. 2021) to validate that detected SiR signals corresponded to HIV-1 particles. Labeled particles could be visualized by spinning disc confocal microscopy (SDCM) in the cellular environment (Figure 3 – figure supplement 1). Confocal images revealed punctate SiR signals in the cytosol, close to the nuclear envelope and within the nucleus of infected cells. Co-localization with CA(IF) staining confirmed that these signals represented entering viral structures (Figure 3a and Figure 3 - figure supplement 2).

Next, TZM-bl cells infected with HIV-1* or HIV-1*CA14^{SiR} were fixed and analyzed for the presence of click labeled subviral particles inside the nucleus at different time points after infection. Consistent with earlier results (Zurnic Bönisch et al. 2020; Burdick et al. 2020; T. G. Müller et al. 2021), we observed nuclear CA(IF) positive foci in HIV-1* infected cells as early as 6 h post infection (Figure 3b, black), while such signals were absent in noninfected cells (Figure 3b, grey). Importantly, we detected SiR positive complexes in the nucleus of HIV-1*CA14^{SiR} infected cells, with the vast majority also positive for CA(IF) (Figure 3b, magenta). Nuclear entry appeared to be delayed for HIV-1*CA14^{SiR} compared to HIV-1* by approximately 12 h. Nevertheless, comparable numbers of cells with detectable capsid-like objects in the nucleus and the number of objects per cell were reached between 12 and 18 h p.i. (Figure 3b and c).

bioRxiv preprint doi: https://doi.org/10.1101/2021.09.14.460218; this version posted September 14, 2021. The copyright holder for this preprint (which was not certified by peer review) is the author/funder, who has granted bioRxiv a license to display the preprint in perpetuity. It is made available under aCC-BY 4.0 International license.

At 12 h p.i., HIV-1*CA14^{SiR} reached the highest number of nuclear particles per cell, with an average of 4.58 ± 4.12, similar to HIV-1* with 5.91 ± 4.11.

Delayed detection of subviral complexes in the nucleus may be due to slower uptake, slower trafficking towards the nuclear envelope, delayed passage through the NPC, or a combination thereof. In order to distinguish between these possibilities, we extended the time-resolved quantification to objects in close vicinity to the nuclear envelope (Figure 3d). This analysis revealed that the HIV-1*CA14^{SiR} derived subviral structures reached the nuclear envelope with similar kinetics to HIV-1* particles (Figure 3d, NE assoc.). A comparable average proportion of CA containing objects was detected at the nuclear envelope in both cases at 6 h, while the numbers of nuclear capsids were lower for HIV-1*CA14^{SiR} at that time (Figure 3d, Nucleus). In contrast, the highest proportion of HIV-1*CA14^{SiR} nuclear objects with 4.20 ± 1.80% was detected at 18 h p.i., while HIV-1* reached similar levels already at 6 h p.i. We conclude that uptake and intracellular trafficking of HIV-1*CA14^{SiR} complexes occurs with similar efficiency as for the wt virus, but transport into the nucleus is slower, offering a possible explanation for the slightly reduced infectivity of HIV-1*CA14^{SiR} virions. This implies that the mechanistic action of the capsid in nuclear import underlies tight margins with respect to its biophysical properties.

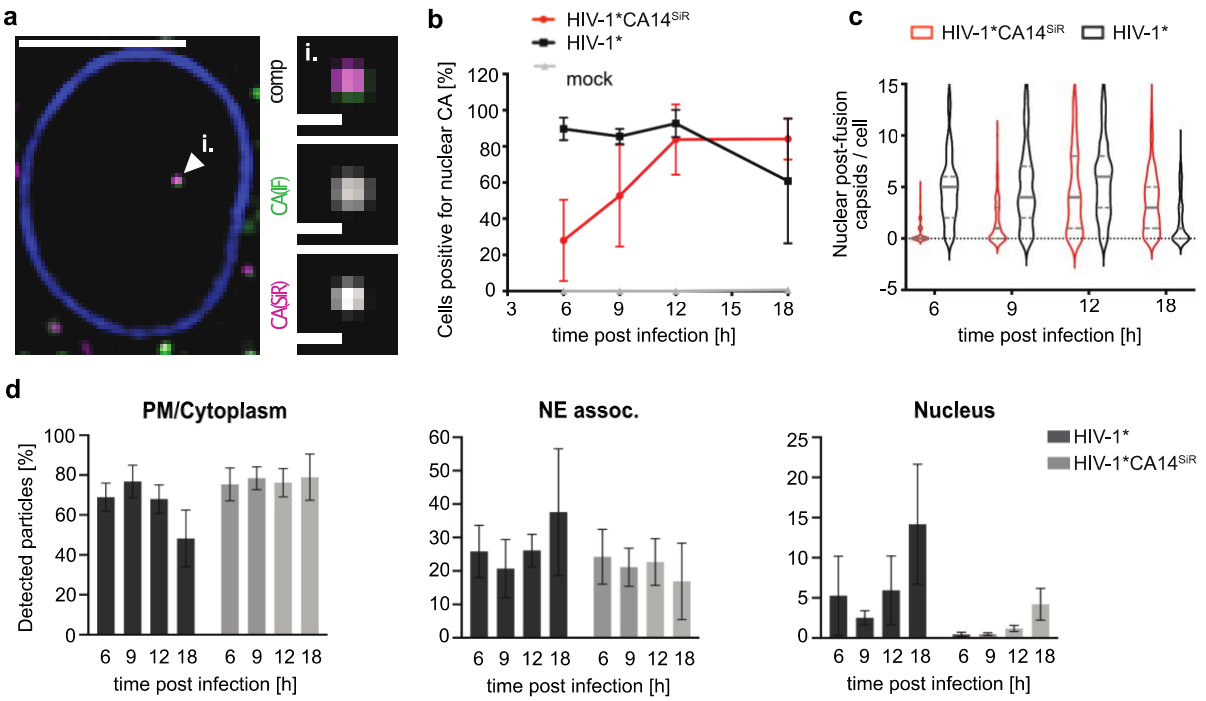

bioRxiv preprint doi: https://doi.org/10.1101/2021.09.14.460218; this version posted September 14, 2021. The copyright holder for this preprint (which was not certified by peer review) is the author/funder, who has granted bioRxiv a license to display the preprint in perpetuity. It is made available under aCC-BY 4.0 International license.

Figure 3. Detection of CA in the nucleus of infected HeLa-derived cells. TZM-bl cells were infected with HIV-1* or HIV-1* CA14^{SiR} particles (~MOI 0.8), treated with 15 µM PF74 for 1 h, fixed at 6, 9, 12 and 18 h p.i. and imaged by SDCM. **(a)** Single z slice of a representative cell infected with HIV-1* CA14^{SiR} at 18 h p.i. and one enlarged z slice are shown. Scale bars: 10 µm (cell) and 1 µm (enlargement). Mean filter and background subtraction was applied for clarity. The image shows a representative image from one of three independent experiments. See Figure 3-figure supplement 1 and 2 for additional data. **(b-d)** Infection time course of click labeled HIV-1* CA14^{SiR} compared to HIV-1*. **(b)** Quantification of cells positive for nuclear CA positive objects over time post infection for HIV-1* (black; CA(IF)), HIV-1* CA14^{SiR} (red; CA(IF)/CA(SiR)) and noninfected control (grey; CA(IF)). Mean values and SD from three independent experiments are shown (n>115 cells per timepoint). **(c)** Number of nuclear CA foci per cell determined for cells infected with HIV-1* (black) or HIV-1* CA14^{SiR} (red) at the indicated timepoints. n>120 cells were analyzed per sample. The median and quartile lines are indicated in grey. **(d)** Localization of particles within a cell for HIV-1* (dark grey) and HIV-1* CA14^{SiR} (light grey). The proportion of total particles per cell detected at the PM or in the cytoplasm (= PM/cytoplasm) at the nuclear envelope (=NE associated) or inside the nucleus was determined at the indicated time points. Data from two of three independent experiments are shown. n>20 cells were analyzed per time point, and error bars represent the SD of the mean.

Characterization of nuclear CA^{SiR} containing complexes

A long-standing question in the field of HIV-1 early replication is the question of when and where capsid uncoating takes place. The possibility to directly detect CA molecules clicked to a synthetic fluorophore enabled us to assess the amounts of CA associated with subviral complexes at different intracellular sites, without the influence of differential epitope accessibility or of a tag domain that potentially confers different properties to a subpopulation of CA molecules. Nevertheless, comparing labeling intensities for nuclear, cytoplasmic, and extracellular particle-associated structures may be confounded in diffraction-limited microscopy by the failure to resolve closely adjacent individual capsids. Clusters of nuclear capsids had indeed been observed by CLEM analyses in our previous study (T. G. Müller et al. 2021).

bioRxiv preprint doi: https://doi.org/10.1101/2021.09.14.460218; this version posted September 14, 2021. The copyright holder for this preprint (which was not certified by peer review) is the author/funder, who has granted bioRxiv a license to display the preprint in perpetuity. It is made available under aCC-BY 4.0 International license.

To determine whether nuclear cluster formation occurred under our conditions, we exploited the fact that the chemical dye conjugated to the capsid surface renders the modified virus suitable for super-resolution microscopy. With a lateral resolution of <50 nm, STED nanoscopy allows visual separation of closely adjacent CA objects. TZM-bl cells were infected with HIV-1*CA14^{SiR} at two different MOIs. An MOI of ~0.8 corresponded to the conditions generally used in our experiments; a 10-fold higher virus dose (MOI ~8) was applied in a parallel experiment to potentially enhance capsid clustering. At 18 h p.i., cells were fixed, immunostained against CA, and imaged using a STED system in confocal and STED mode (Figure 4). Nuclear CA(IF)/(SiR) double-positive objects were detected under both conditions (Figure 4a, arrowheads). While these objects appeared as individual punctae in diffraction-limited micrographs from the IF and SiR channels at both MOIs (Figure 4b, top and middle row), imaging of the SiR channel in STED mode revealed differences between individual punctae. Some diffraction-limited punctae in the nucleus represented individual capsid-like objects when imaged by STED (Figure 4b, left panel, bottom row). In contrast, other punctae were resolved into small clusters of 2-4 closely apposed CA-containing objects by super-resolution microscopy (Figure 4b, right, bottom panel), consistent with observations made by electron tomography (T. G. Müller et al. 2021; Zila et al. 2021). A quantitative analysis of cluster sizes (Figure 4c) revealed that the propensity for capsid clustering in the nucleus correlated with the amount of virus used for infection: at an MOI~0.8, the vast majority of punctae (~88%) corresponded to individual capsid-like objects in the nucleus, and clusters of more than two objects were not observed. On the other hand, almost half of the nuclear punctae (~43%) corresponded to clusters of 2-4 objects when cells were infected with the high MOI~8. We conclude that nuclear capsid clustering is rarely observed at the MOI of 0.8 used throughout this study. The previously observed capsid clustering in distinct nuclear positions appears to occur preferentially at high MOI.

bioRxiv preprint doi: https://doi.org/10.1101/2021.09.14.460218; this version posted September 14, 2021. The copyright holder for this preprint (which was not certified by peer review) is the author/funder, who has granted bioRxiv a license to display the preprint in perpetuity. It is made available under aCC-BY 4.0 International license.

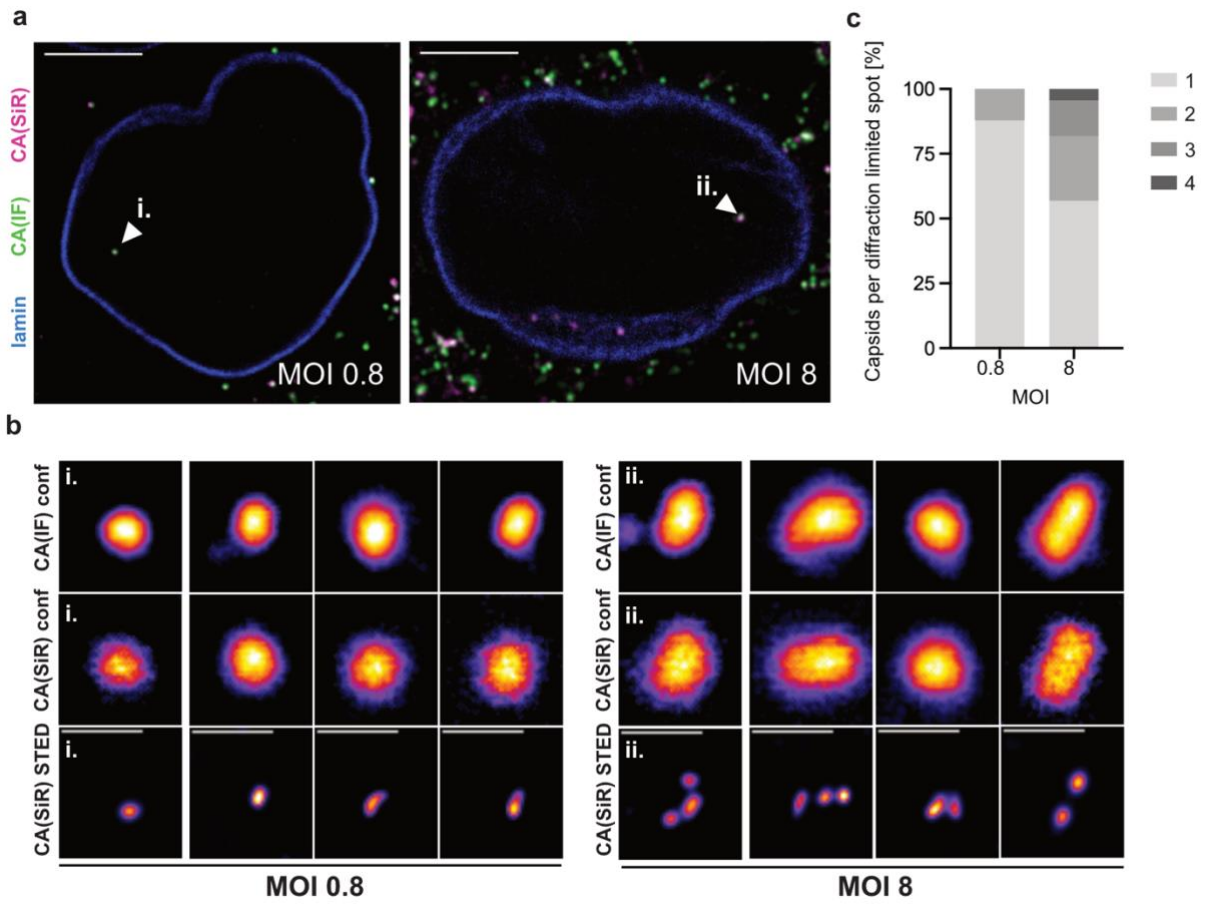

Figure 4. Dose-dependent clustering of nuclear capsids in HeLa-derived cells. TZM-bl cells were infected with HIV-1* CA14^{SiR} at the indicated MOI for 18 h, treated with 15 µM PF74 for 1 h, immunostained against CA (green) and lamin A (blue) and imaged using an Abberior STED setup. Mean filter and background subtraction was applied to all images for clarity. **(a)** Micrographs of TZM-bl cells infected with an MOI ~0.8 (left) or MOI ~8 (right). Arrowheads indicate nuclear CA(IF)/CA(SiR) positive objects shown enlarged in (b). Scale bars: 10 µm. **(b)** Representative images of nuclear CA containing objects from cells infected with a low MOI (MOI~0.8, left panel) or a high MOI (MOI~8, right panel). CA(IF) and CA(SiR) were imaged in confocal mode (top and middle row, respectively). CA(SiR) images were also recorded in STED mode (bottom row). The figure shows four representative foci each from one of two individual experiments. Mean filter and background subtraction were applied. Scale bars: 500 nm. **(c)** Diffraction-limited nuclear foci were analyzed by STED nanoscopy in cells infected with an MOI~0.8 (n = 33) and an MOI~8 (n =44) and classified by the number of individual capsids per focus.

bioRxiv preprint doi: https://doi.org/10.1101/2021.09.14.460218; this version posted September 14, 2021. The copyright holder for this preprint (which was not certified by peer review) is the author/funder, who has granted bioRxiv a license to display the preprint in perpetuity. It is made available under aCC-BY 4.0 International license.

We next proceeded to SiR fluorescence intensity measurements, comparing the signal intensity of extranuclear HIV-1 particles to that of subviral structures in the nucleus. Staining of the plasma membrane with mCling before infection revealed that under our conditions most cell-associated particles in the cytosolic region represented virions present in endosomes, corresponding to a pre-fusion state of the virus (Figure 5 – figure supplement 1). To ensure that these extranuclear punctae represented single objects, cytoplasmic foci were analyzed in STED mode. We found that ~95% (n=79) of analyzed objects corresponded to an individual object, while only ~5% (n=4) of these foci were resolved into two objects by nanoscopy (Figure 5 – figure supplement 2). As illustrated by the cartoon in Figure 5a, complete virions comprise on average ~2,400 CA molecules, while only ~1,200-1,500 of these are part of the mature fullerene capsid (John A.G. Briggs et al. 2003; Carlson et al. 2008; Lanman et al. 2004) that represents a post-fusion state. Assuming equal click labeling efficiency of CA14^{ncAA} for molecules that are part of the mature lattice and those that remain free in the viral volume, the average SiR intensity of complete capsids would be expected to correspond to ~60% of the average intensity of complete virions from the same preparation. We infected TZM-bl cells at an MOI of 0.8 and quantified the SiR intensity of >6,000 virions attached to the cell or in the cytosolic region and of >100 nuclear punctae. The average SiR intensity of cell-attached and (mostly) endosomal particles in the cytosolic region exhibited an average of 17,649 a.u.. In contrast, the SiR intensity of nuclear subviral structures averaged 9,835 a.u. (Figure 5b), i.e., ~56% of the average intensity of complete virions, in line with the predicted relative CA content of the mature capsid. Based on these findings, we conclude that the CA(SiR) containing objects in the nuclei of these cells correspond approximately to a full complement of the mature capsid.

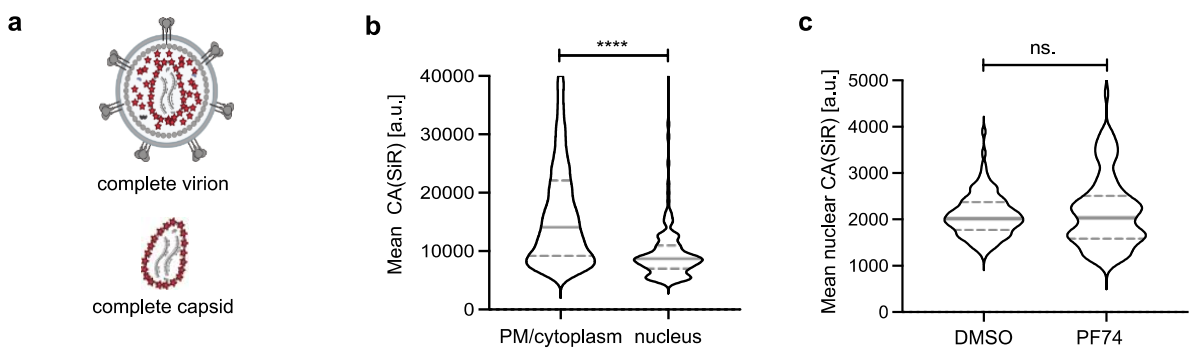

bioRxiv preprint doi: https://doi.org/10.1101/2021.09.14.460218; this version posted September 14, 2021. The copyright holder for this preprint (which was not certified by peer review) is the author/funder, who has granted bioRxiv a license to display the preprint in perpetuity. It is made available under aCC-BY 4.0 International license.

Figure 5. Largely intact capsids are detected in the nucleus of HeLa-derived cells. TZM-bl cells were infected with HIV-1* or HIV-1*CA14^{SiR} (MOI~0.8), treated with 15 µM PF74 for 1 h before fixation at the indicated time points and imaged by SDCM. **(a)** Scheme of the relative CA content in complete virions (~ 2,400 CA) on glass/plasma membrane or in endosomes in the cytosol. Post-fusion capsids contain only the CA molecules incorporated into the mature capsid lattice (~ 1,500 CA). Image created with BioRender **(b)** Quantification of CA(SiR) intensities associated with CA(IF) positive objects at the indicated localizations. Data from three independent experiments are shown. Cells from seven fields of view were analyzed ($n_{particles}$= 6441 PM/cytoplasm, 135 nucleus). Lines indicate median values (PM/cytoplasm: 17,649.22 ± 11,663.47; nucleus: 9,835.08 ± 5,708.14) and interquartile range. Significance was determined by two-tailed Student`s t-test (*** < 0.001). **(c)** Quantification of CA(SiR) intensities of nuclear objects. TZM-bl cells were treated with DMSO or 15 µM PF74 for 1 h prior fixation at 17 h p.i.. Lines indicate median values (DMSO: 2,086.83 ± 456.35, n=100; PF74: = 2,164.51 ± 783.45, n=100) and interquartile range. Significance was determined by two-tailed Student`s t-test (n.s. >0.05).

The small molecule inhibitor PF74 (Blair et al. 2010) binds to the HIV-1 capsid in a pocket overlapping the binding sites for the FG motifs of various nucleoporins and for the nuclear host protein CPSF6; the compound inhibits HIV-1 replication by multiple mechanisms (McArthur et al. 2019; Novikova et al. 2019; Thenin-Houssier and Valente 2016). Treatment with high concentrations of PF74 has been reported to destabilize the capsid (Shi et al. 2011; Price et al. 2014; Blair et al. 2010; Pornillos et al. 2010; Lee et al. 2012; Yang Yang, Luban, and Diaz-Griffero 2014), but data that we had obtained using CA(IF) detection argued against a PF74 induced loss of CA from nuclear complexes (T. G. Müller et al. 2021). Since we cannot exclude that results obtained by immunodetection are influenced by differential CA epitope exposure, we re-addressed this issue employing direct CA labeling. TZM-bl cells were infected with HIV-1*CA14^{SiR} particles for 17 h and treated with 15 µM PF74 or DMSO for 1 h, followed by fixation, permeabilization, methanol extraction, and SDCM imaging. As shown in Figure 5c, CPSF6 was removed from the subviral complexes, in accordance with earlier results (T. G. Müller et al. 2021). In contrast, mean CA(SiR) intensity remained unaltered, indicating that the capsid remains largely stable under these conditions.

Detection of directly labeled HIV-1 capsids in primary cells

bioRxiv preprint doi: https://doi.org/10.1101/2021.09.14.460218; this version posted September 14, 2021. The copyright holder for this preprint (which was not certified by peer review) is the author/funder, who has granted bioRxiv a license to display the preprint in perpetuity. It is made available under aCC-BY 4.0 International license.

To validate our results in a physiologically relevant cell type, primary human CD4$^+$ T cells from healthy blood donors were infected, subjected to IF staining against CA, and imaged by SDCM at 24 h p.i. (Figure 6a and Figure 6 – figure supplement 1). We readily detected nuclear subviral SiR positive structures in HIV-1*CA14^{SiR} infected cells, indicating that nuclear replication complexes retained CA also in these primary cells (Figure 6a). Consistent with prior observations made in this cell type (Zila et al. 2019), the majority of SiR-positive objects were not associated with CA(IF) signals (9/11 particles; Figure 6a, left) when fixation and immunostaining were performed under standard conditions. As outlined above, treatment with 15 µM PF74 for 1 h dissociates the large clusters of CPSF6 from nuclear subviral complexes. We observed that this in turn renders nuclear CA accessible for IF detection in T cells, presumably by exposure of CA epitopes upon CPSF6 displacement (T. G. Müller et al. 2021). Accordingly, brief PF74 treatment allowed for detection of CA(IF) signals co-localizing with nuclear CA(SiR) punctae (13/16; Figure 6a, right). We conclude that the direct CA labeling strategy presented here overcomes technical artifacts that hamper IF analyses.

Further quantitative analyses using primary CD4$^+$ T cells prepared from six blood donors revealed similar numbers of nuclear capsid structures in cells infected with HIV-1*CA14^{SiR} than in cells infected with HIV-1* at 24 h p.i. (Figure 6b). SiR intensity measurements were only performed for intranuclear objects in this case since high background due to SiR accumulation in the narrow cytoplasm of T cells precluded reliable analysis of individual particles in the extranuclear region (see Figure 6a and Figure 6 – figure supplement 1). Quantitation of SiR intensities of nuclear punctae in cells infected with an MOI~0.8 yielded similar average intensities as measured in TZM-bl cells (mean=12,485 a.u.), indicating the presence of a complete or nearly complete mature capsid in the nuclear complexes in primary T cells (Figure 6c). Cells infected with an MOI of ~8 displayed higher CA(SiR) intensities of diffraction-limited nuclear objects (mean=39,502 a.u.), suggesting intranuclear clustering of capsids, as observed in TZM-bl cells (Figure 4).

Our findings from CA(SiR) intensity measurements argue for the presence of a full capsid complement at subviral structures in the nucleus. These data strengthen conclusions from several recent studies suggesting that the mature capsid lattice may be completely or largely intact on nuclear subviral objects (T. G. Müller et al. 2021; Burdick et al. 2020; Selyutina et al. 2020). However, fluorescence signals do not yield

bioRxiv preprint doi: https://doi.org/10.1101/2021.09.14.460218; this version posted September 14, 2021. The copyright holder for this preprint (which was not certified by peer review) is the author/funder, who has granted bioRxiv a license to display the preprint in perpetuity. It is made available under aCC-BY 4.0 International license.

information on the architecture of nuclear CA14^{SiR} containing objects. Therefore, we complemented our analyses by performing CLEM of infected SupT1 T cells. In order to maximize the number of nuclear objects, infection was synchronized by the attachment of particles to the cells for 3 h at a low temperature (16°C) to prevent particle uptake by membrane fusion or endocytosis (Weigel and Oka, 1981; Melikyan *et al.*, 2000). Virus entry was then initiated by temperature shift to 37°C (Zila et al. 2019). At 24 h post temperature shift, specimens were prepared by high-pressure freezing (HPF) and freeze substitution, and 250 nm thick resin sections were subjected to SDCM in order to localize CA(SiR) containing structures, followed by correlative electron tomography (CLEM-ET) analysis. CA(SiR) positive objects could be identified by SDCM in the sections (Figure 6d), demonstrating that the brightness of signals derived from direct CA(SiR) labeling is sufficient for CLEM detection of cytosolic and nuclear (sub)viral structures. ROIs were defined based on the SiR signals and subjected to correlative ET analysis. Figure 6e shows an exemplary tomogram obtained from a ROI located within the nucleus. It reveals several closely attached electron-dense structures at the position of the SiR label, whose shape and dimension match those of intact or largely intact mature HIV-1 capsids (Figure 6f and supplementary movie 1). Such structures were recently identified in nuclei of infected cells by CLEM using fluorescently labeled HIV-1 IN as an indirect marker for subviral structures (Zila et al. 2021; T. G. Müller et al. 2021) and were interpreted as capsid shells based on their morphology. Here we demonstrate that such structures co-localize with nuclear foci comprising a high number of click labeled CA molecules, thereby providing direct evidence that the cone-shaped objects are HIV-1 capsids that have entered the nucleus of infected cells.

bioRxiv preprint doi: https://doi.org/10.1101/2021.09.14.460218; this version posted September 14, 2021. The copyright holder for this preprint (which was not certified by peer review) is the author/funder, who has granted bioRxiv a license to display the preprint in perpetuity. It is made available under aCC-BY 4.0 International license.

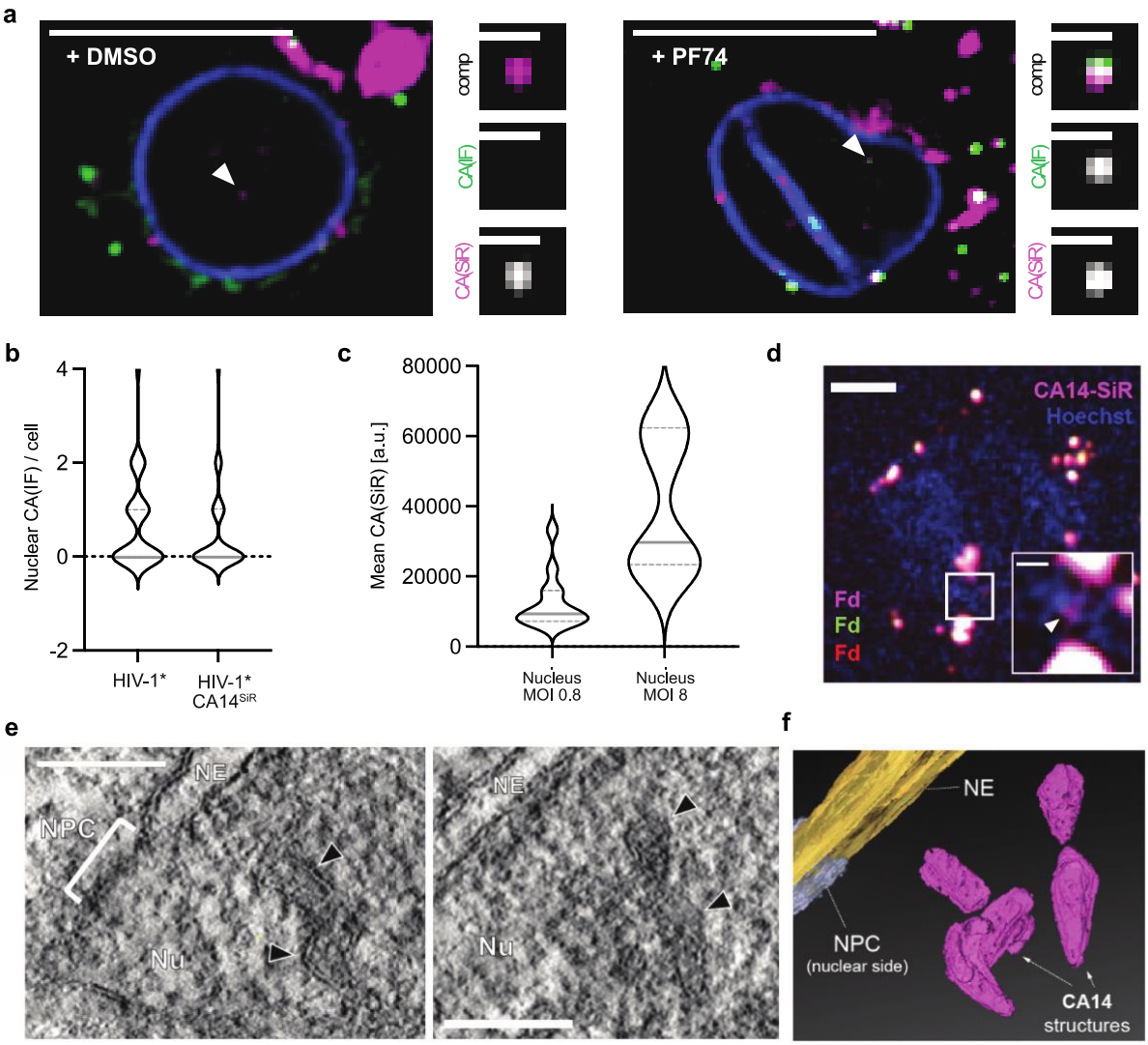

548

549 **Figure 6 Largely complete click labeled capsid structures detected in the**
550 **nucleus of primary CD4⁺ T cells and T cell line. (a)** Activated CD4⁺ T cells were
551 infected with HIV-1*CA14^{SiR} (MOI~0.8) for 24 h before DMSO/PF74 treatment for 1 h,
552 fixation, and methanol extraction. Samples were immunostained against CA (green)
553 and laminA (blue). Images show a single z slice through the cell. Enlargements show
554 the particle marked by the arrowhead. Scale bars: 10 µm (overview) and 1 µm
555 (enlargement). **(b)** Data analyzed from the experiment outlined in (a). The graph shows
556 the number of CA positive foci per nucleus in cells infected with HIV-1* (n=35 cells,
557 mean=0.85) or HIV-1*CA14^{SiR} (n= 73 cells, mean=0.51). Pooled data from 6 different
558 blood donors are shown. Grey lines show median and interquartile lines. **(c)** CA(SiR)
559 intensities of nuclear objects in infected and activated CD4⁺ T cells at an MOI~0.8
560 (n=13; mean=12,485 ± 7,445 a.u.) and an MOI ~8 (n=7; mean=39,502 ± 18,025 a.u.).
561 MOI was determined in TZM-bl cells. Grey lines show median and interquartile lines.
562 **(d-f)** Nuclear cone-shaped capsids detected by CLEM-ET. SupT1 cells were treated

bioRxiv preprint doi: https://doi.org/10.1101/2021.09.14.460218; this version posted September 14, 2021. The copyright holder for this preprint (which was not certified by peer review) is the author/funder, who has granted bioRxiv a license to display the preprint in perpetuity. It is made available under aCC-BY 4.0 International license.

with 1 µM aphidicolin (APC) for 16 h to prevent cell division, before infection with HIV-1*CA14^{SiR} virions (2.3 µU RT/cell, corresponds to an MOI~0.4 determined in TZM-bl cells). At 24 h p.i., cells were cryo-immobilized by high-pressure freezing, freeze substituted, and further processed for CLEM and ET as described in materials and methods. **(d)** SDCM image of a 250-nm thick resin section of the cell infected with HIV-1*CA14^{SiR} virions (magenta), post-stained with Hoechst (blue) and decorated with multi-fluorescent fiducials (Fd) for correlation. The arrowhead in the enlargement of the boxed region indicates a CA(SiR) signal within the Hoechst-stained nuclear region. Scale bars: 1 µm (overview) and 200 nm (enlargement). **(e)** Computational slices through tomographic reconstructions at the correlated region boxed in (d) with views highlighting the presence of clustered capsid-reminiscent structures (black arrowheads) in the nuclear region. Nu, nucleus; NPC, nuclear pore complex; NE, nuclear envelope. Scale bar: 100 nm. **(f)** Segmented and isosurface rendered structure of the cones detected in (e). Magenta: capsid, yellow: NE, cyan: NPC. See also supplementary movie 1.

Discussion

Here we present a direct labeling approach for the HIV-1 CA protein that yields infectious and morphologically mature viral particles. The minimally invasive GCE / click labeling approach used here represents an ideal strategy for the versatile labeling of genetically fragile viral capsid proteins. Its potential for virus imaging has not been exploited, however, presumably because this method is still challenging in eukaryotic cells. While GCE has been explored in virology for the generation of conditionally replication-competent live attenuated vaccines (Yuan et al. 2017; Si et al. 2020; Wang et al. 2014), the combination of GCE and click labeling for the purpose of capsid imaging has only been successfully applied for the non-enveloped adeno-associated virus (AAV) (Zhang et al. 2018; Seo et al. 2020; Katrekar et al. 2018; Rubino et al. 2012). Unlike HIV-1 CA, the AAV capsid protein has also been shown to tolerate modifications by peptide insertions (Asokan, Schaffer, and Samulski 2012; Kotterman and Schaffer 2014; Thadani et al. 2018; Börner et al. 2020; Grimm and Zolotukhin 2015). Here, we demonstrate that GCE in conjunction with click labeling can also be applied to an enveloped virus with a highly multifunctional and extremely genetically fragile capsid protein. In contrast to other genetic tagging strategies described, the

bioRxiv preprint doi: https://doi.org/10.1101/2021.09.14.460218; this version posted September 14, 2021. The copyright holder for this preprint (which was not certified by peer review) is the author/funder, who has granted bioRxiv a license to display the preprint in perpetuity. It is made available under aCC-BY 4.0 International license.

minimally invasive approach allows labeling of HIV-1 CA without requiring complementation with wt virus.

The detection of a chemical fluorophore covalently attached to CA is independent of cellular context, sample treatment, or exposure of CA epitopes. Thereby, the approach overcomes limitations of IF detection that had previously led to different conclusions regarding the presence of HIV-1 CA at nuclear subviral complexes. CA amounts roughly corresponding to a full complement of a mature capsid were found to be associated with subviral complexes in the nuclei of a HeLa-derived cell line and primary human $CD4^+$ T cells, also upon inhibition of cell division by aphidicolin treatment. These findings support recent reports from us and others, which indicated that the nuclear pore channel is wider than assumed earlier, allowing HIV-1 capsids to pass the intact NPC, and that uncoating occurs after nuclear import (T. G. Müller et al. 2021; Zila et al. 2021; Selyutina et al. 2020; Dharan et al. 2020; Francis, Marin, Singh, et al. 2020; Burdick et al. 2020; Chen et al. 2016).

The HIV-1 capsid is the largest structure reported to pass through a nuclear pore to date, and cryo-ET reconstructions of NPCs in situ indicate that the NPC opening has a similar diameter to the broad end of the capsid (Zila et al. 2021). The HIV-1 capsid might thus represent the upper limit of NPC cargo size, so the addition of substantial molecular mass to its surface may block nuclear import. Our data show the site-specific introduction of a small molecule (molecular mass of SiR: 614.8 Da) into CA, at a position distant from the FG-binding pocket involved in interaction with nucleoporins and CPSF6, is tolerated by HIV-1. However, we did observe a delay in nuclear import that might be due to the additional mass and/or altered surface properties of the modified capsid. This will be a topic of further study.

Due to the use of synthetic dye molecules, the labeling strategy presented is compatible with a wide range of fluorescence imaging approaches, including live-cell microscopy, correlative imaging and super-resolution fluorescence microscopy techniques (i.e., STED (Klar and Hell 1999), dSTORM (Heilemann et al. 2008), and Minflux (Balzarotti et al. 2017)). By applying correlative imaging, we could provide direct evidence that capsid-shaped objects, as recently detected in the nucleus by correlative ET before as well as after separation of the viral genome from the bulk of viral proteins (T. G. Müller et al. 2021; Zila et al. 2021), indeed represent HIV-1 capsids or capsid-like remnants. Our observations are in apparent contrast to findings from

bioRxiv preprint doi: https://doi.org/10.1101/2021.09.14.460218; this version posted September 14, 2021. The copyright holder for this preprint (which was not certified by peer review) is the author/funder, who has granted bioRxiv a license to display the preprint in perpetuity. It is made available under aCC-BY 4.0 International license.

other recent fluorescence imaging-based studies that reported uncoating directly before or during passage of the capsid through the NPC (Mamede et al. 2017; Burdick et al. 2017; Francis et al. 2016; Francis and Melikyan 2018; Fernandez et al. 2019; Rasaiyaah et al. 2013; Arhel et al. 2007; Hulme, Perez, and Hope 2011; Zurnic Bönisch et al. 2020; Lukic et al. 2014; Y. Yang, Fricke, and Diaz-Griffero 2013), or a very rapid loss of the CA signal following nuclear uncoating (Burdick et al. 2020). These apparent discrepancies might be explained by different capsid labeling strategies. Loss of the capsid signal at the nuclear pore was observed when a tagged variant of the CA binding protein CypA was used as an indirect capsid marker (Francis et al. 2016; Francis and Melikyan 2018). It is conceivable that the marker protein could be displaced by Nup358, which also binds to the CypA binding loop in CA (Schaller et al. 2011), at the outer ring of the nuclear pore. Rapid nuclear dissociation of the CA signal was observed upon incorporating a small proportion of eGFP-tagged CA as a capsid marker (Zurnic Bönisch et al. 2020; Burdick et al. 2020). In this case, CA molecules modified by a relatively large tag might alter the stability of the capsid or dissociate more rapidly from the viral structure than the native protein. We believe that the data obtained by correlative microscopy taken together argue that HIV-1 uncoating is not accompanied by rapid capsid disassembly, but rather occurs via separation of the viral genome from a broken capsid remnant (T. G. Müller et al. 2021). Combining the direct CA labeling described here with the recently developed fluorescence detection of the reverse transcribed genome (Blanco-Rodriguez et al. 2020; T. G. Müller et al. 2021) will provide us with the possibility to study the uncoating process in more detail using a combination of confocal imaging, nanoscopy, and correlative imaging.

STED nanoscopy allowed us to perform a more detailed analysis of the punctuate CA(SiR) signals within the cell by differentiating between individual CA foci and clusters of closely adjacent capsid-like objects. The vast majority (>95%) of individual CA^{SiR} punctae detected in the cytosolic area of HeLa-derived model cells represented virions in endosomes, as determined by co-staining with a fluorescent membrane marker. This observation is consistent with efficient Env and receptor-independent endocytic uptake of HIV-1 into HeLa cells due to a high density of heparan sulfate at the plasma membrane (Marsh and Helenius 2006; Permanyer, Ballana, and Esté 2010; Gregory B. Melikyan 2014). In the nucleus, we observed small clusters of capsid-like objects upon high MOI infection, as we and others have recently described (Francis, Marin, Singh, et al. 2020; T. G. Müller et al. 2021; Rensen et al. 2021). Our analyses revealed

bioRxiv preprint doi: https://doi.org/10.1101/2021.09.14.460218; this version posted September 14, 2021. The copyright holder for this preprint (which was not certified by peer review) is the author/funder, who has granted bioRxiv a license to display the preprint in perpetuity. It is made available under aCC-BY 4.0 International license.

that this clustering is dependent on the amount of virus used for infection. Most nuclear signals represented single capsids at a lower MOI, whereas frequent clustering was observed at high MOI. These findings suggest that capsids enter the nucleus individually, but traffic via a limited number of routes to accumulate at defined sites of uncoating. This raises the question of whether HIV-1 uses a 'specialized' subset of nuclear pores for nuclear entry; the answer would not only be of interest in the context of HIV-1 replication, but also with respect to an understanding of the nuclear import process. Nup levels and presumably NPC composition have been found to influence HIV-1 replication (Kane et al. 2018), but the compositional and structural variability of NPCs between different cell types, or within an individual cell, is incompletely understood (reviewed in Knockenhauer and Schwartz, 2016). Nuclear speckles were recently identified as HIV-1 uncoating sites, with trafficking to these sites presumably guided by CPSF6 (Selyutina et al. 2020; Francis, Marin, Singh, et al. 2020; Rensen et al. 2021). Whether nuclear capsid clustering occurs in the context of natural infection - and whether it offers an advantage for virus replication or is simply a byproduct of the HIV-1 nuclear trafficking/uncoating pathway - is unknown. However, high MOI conditions can physiologically be reached by cell-to-cell infection (Sattentau 2010). Hence, the clustering phenotype warrants further investigation.

The direct labeling approach also allowed us to investigate the effect of the capsid inhibitor PF74, whose detailed mode of action and inhibition is still under investigation, on nuclear capsids. While some studies reported an accelerated uncoating with high PF74 concentrations (Blair et al. 2010; Lee et al. 2012; Yang Yang, Luban, and Diaz-Griffero 2014; Pornillos et al. 2010; Shi et al. 2011), others did not observe any dramatic change in capsid core stability (Rankovic et al. 2018; Rasaiyaah et al. 2013; T. G. Müller et al. 2021). Our data indicate that the displacement of CPSF6 from nuclear capsids by a high concentration of PF74 is not accompanied by capsid disassembly, consistent with *in vitro* findings that indicate breakage of lattice integrity by PF74, but stabilization of the remaining lattice (Márquez et al. 2018).

In conclusion, direct click labeling of HIV-1 CA is a versatile approach that significantly expands the possibilities to study the early events in HIV-1 replication with high temporal and/or spatial resolution using advanced fluorescence microscopy methods. Application for the HIV-1 CA provided direct proof that the capsid stays largely intact upon passage of the subviral complex into the nucleus and directly identified nuclear capsid-like structures that morphologically resembled the virion capsid by CLEM-ET.

bioRxiv preprint doi: https://doi.org/10.1101/2021.09.14.460218; this version posted September 14, 2021. The copyright holder for this preprint (which was not certified by peer review) is the author/funder, who has granted bioRxiv a license to display the preprint in perpetuity. It is made available under aCC-BY 4.0 International license.

The fact that the combination of GCE and click chemistry could successfully be applied to a notoriously genetically fragile capsid protein of an enveloped virus opens the perspective that this strategy may also advance and expand fluorescence labeling of a broad range of other viruses.

Acknowledgements

We acknowledge microscopy support from the Infectious Diseases Imaging Platform (IDIP) at the Center for Integrative Infectious Disease Research, Heidelberg. We thank Eyal Arbely (The National Institute for Biotechnology in the Negev, Beer-Sheva, Israel) for providing pEA168. pNESPlyRS-eRF1dn-tRNA was kindly provided by Anna-Lena Schäfer (University Hospital Heidelberg, Heidelberg, Germany).

This work was funded by the Deutsche Forschungsgemeinschaft (DFG; German Research Foundation), Projektnummer 240245660, SFB 1129 project 6 (B.M.) and project 5 (H.G.K.).

Materials and Methods

Reagent type (species) or resource	Designation	Source or reference	Identifiers	Additional information
Antibody	Rabbit polyclonal anti-HIV-1 CA	In-house	N/A	1:1000 IF
Antibody	Mouse monoclonal anti-Lamin A/C	Santa Cruz Biotechnology	RRID:AB_627875; Cat# sc-7292	1:100 IF; works for HeLa cells and MDM
Antibody	Mouse monoclonal anti-LaminB1	Santa Cruz Biotechnology	Cat# sc-365962	1:200 IF; works for SupT1 and primary $CD4^+$ T cells
Antibody	Sheep polyclonal anti-HIV-1 CA	(Müller et al., 2009)	N/A	1:5000
Antibody	Rabbit polyclonal anti-HIV-1 RT	(Müller et al., 2004)	N/A	1:1000
Antibody	Rabbit polyclonal anti-HIV-1 MA	In-house	N/A	1:100?
Antibody	Alexa Fluor (405, 488, 568 and 647) secondary antibodies	Thermo Fisher Scientific	N/A	1:1000 IF
Antibody	sheep IgG, IRDye 680RD conjugated	LI-COR Biosciences	RRID:AB_10954442	1:10000
Antibody	rabbit IgG, IRDye 800CW conjugated	LI-COR Biosciences	RRID:AB_621848	1:10000
Antibody	Goat anti-mouse IgG conjugated with STAR ORANGE	Abberior GmbH	RRID:AB_2847853	1:200 STED
Cell line (*H. sapiens*)	Hela TZM-bl	(Wei et al. 2002)	RRID:CVCL_B478	N/A
Cell line (*H. sapiens*)	Embryonic kidney 293 T cells (HEK293T)	(Pear et al. 1993)	RRID:CVCL_0063	N/A
Cell line (*H. sapiens*)	Human $CD4^+$ T lymphoblast cells SupT1	(Smith et al. 1984)	RRID:CVCL_1714	N/A
plasmid	HIV-1_{NLC4-3}	(Bohne and Kräusslich 2004)	N/A	HIV-1 proviral plasmid
plasmid	eRF1-E55D	(Schmied et al. 2014)	N/A	Dominant version of eRF1

bioRxiv preprint doi: https://doi.org/10.1101/2021.09.14.460218; this version posted September 14, 2021. The copyright holder for this preprint (which was not certified by peer review) is the author/funder, who has granted bioRxiv a license to display the preprint in perpetuity. It is made available under aCC-BY 4.0 International license.

plasmid	pEA168	(Cohen and Arbely 2016)	N/A	N/A
plasmid	$tRNA^{Pyl}$/$NESPylRS^{AF}$	(Nikić et al. 2016)	N/A	Modified pyrrolysine tRNA sythetase
plasmid	pNESPlyRS-eRF1dn-tRNA	Schifferdecker, Sakin et al. in preparation	N/A	Amber suppression components
plasmid	HIV-1*	This study	N/A	pNLC4-3*
plasmid	HIV-1*$CA14^{TAG}$	This study	N/A	pNLC4-3*CA^{TAG}
plasmid	pcDNA3.1$^{(+)}$	Thermo Fisher Scientific	Cat#V79020	Mammalian expression vector
Chemical	Paraformaldehyde (PFA)	Electron Microscopy Sciences	Cat#15700	16% aqueous solution
Chemical	SiR-tetrazine	Spirochrome	Cat#SC008	1 mM stock in DMSO, -80°C
Chemical	Cyclopropene-L-Lysine (CP)	SiChem	Cat#SC-8017	100 mM in 0.2M NaOH+15% DMSO; -80°C
Chemical	Ascorbic Acid	Sigma Aldrich	Cat#A92902	10 mM in ddH_2O; -20°C
Chemical	mCLING.ATTO488	Synaptic Systems	Cat#710006AT3	Membrane probe, 50µM in ddH_2O; -80°C
Chemical	Enfuvirtide (T-20)	Roche	NIH AIDS Reagent Program Cat#4624	Fusion inhibitor, 20mM in ddH_2O; -20°C
Chemical	PF 3450074 (PF74)	Sigma Aldrich	Cat#SML0835	10 mM in DMSO; -20°C
Chemical	Hoechst33258	Merck	Cat#94403	1:1000
Chemical	Polyethylenimine (PEI)	Merck	Cat#408727	Slide coating; 1mg/ml
Chemical	TetraSpeck beads	Thermo Fisher Scientific	Cat#T7279	
Chemical	Aphidicolin	Merck	Cat#178273	Cell cycle arrest
Software, algorithm	Fiji 1.53c	(Schindelin et al. 2012)	RRID:SCR_002285	General image analysis
Software, algorithm	Icy 2.0.3.0	(De Chaumont et al. 2012)	RRID:SCR_010587	Intensity quantification,
Software, algorithm	Prism 8	GraphPad Software Inc. (CA, United States)	RRID:SCR_002798	Visualization and Plotting
Software, algorithm	Seaborn 0.10.0	(Waskom M et al. 2020)	RRID:SCR_018132	Visualization and Plotting
Software, algorithm	Volocity 6.3	Perkin Elmer (United States)	RRID:SCR_002668	Data acquisition
Software, algorithm	Imaris 9.7.2	Bitplane AG (CHE)	RRID:SCR_007370	Spot detection, Intensity quantification
Software, algorithm	Huygens Professional Deconvolution	SVI (NLD)	RRID:SCR_014237	Deconvolution
Software, algorithm	eC-CLEM (Icy plugin; v 1.0.1.5)	(Paul-Gilloteaux et al. 2017)	http://icy.bioimageanalysis.org/plugin/ec-clem/	Post-correlation
Software, algorithm	SerialEM 3.7.9	(Mastronarde 2005)	RRID:SCR_017293	Tomogram acquisition, Pre-correlation
Software, algorithm	IMOD 4.9.4	(Kremer, Mastronarde, and McIntosh 1996)	RRID:SCR_003297	Tomogram reconstruction
Software, algorithm	Amira 2019.3	Thermo Fisher Scientific	RRID:SCR_007353	Visualization and rendering

List of primers

primer	sequence
Vpr_{TGA} fwd	GGAGCCAGTAGATCCTGAACTAGAGCCCTGGTAC
Vpr_{TGA} rev	GTACCAGGGCTCTAGTTCAGGATCTACTGGCTCC
CA $A14_{BssHII}$ fwd 1	CTTGCTGAAGCGCGCA
CA $A14_{TAG}$ rev 1	AGTTCTAGGTGATATCTACTGATGTACCATTTG

bioRxiv preprint doi: https://doi.org/10.1101/2021.09.14.460218; this version posted September 14, 2021. The copyright holder for this preprint (which was not certified by peer review) is the author/funder, who has granted bioRxiv a license to display the preprint in perpetuity. It is made available under aCC-BY 4.0 International license.

CA $A14_{TAG}$ fwd 2	CAAATGGTACATCAGTAGATATCACCTAGAACT
CA $A14_{ApaI}$ rev 2	GCCCTGCAATTTTTGGCTATGTG

Plasmids

Plasmids were cloned using standard molecular biology techniques and verified by commercial Sanger sequencing (Eurofins Genomics, GER). PCR was performed using Q5 High-Fidelity DNA Polymerase (New England Biolabs, GER) or Phusion DNA Polymerase (New England Biolabs) according to the manufacturer's instructions using primers purchased from Eurofins Genomics. Plasmid amplification was carried out in *E. coli* Stbl2 (Thermo Fisher Scientific, USA) cells.

HIV-1 plasmids were based on the proviral plasmid pNLC4-3 (Bohne and Kräusslich 2004), expressing the authentic genomic RNA from pNL4-3 (Adachi et al. 1986) under the control of the cytomegalovirus promoter. To avoid unwanted ncAA incorporation into the virion component Vpr, the amber stop codon of the *vpr* ORF of pNLC4-3 was mutated into an opal stop codon (TGA) via site-directed mutagenesis. An EcoRI/StuI fragment comprising the *vpr* coding region was subcloned from pNLC4-3 into pcDNA3.1(+) (Thermo Fisher Scientific). Mutagenesis of the *vpr* stop codon was performed using QuikChange Site-Directed Mutagenesis (Liu and Naismith 2008) with overlapping primers including the desired mutation (Vpr_{TGA} fwd and rev), and the mutated fragment was transferred back into pNLC4-3 via EcoRI/StuI, resulting in plasmid pNLC4-3* (HIV-1*).

The amino acid A14 of the CA coding sequence (GCC) was mutated into TAG via overlap PCR to obtain a plasmid suitable for click labeling of the CA protein. PCR1 (primers $CA14_{BssHII}$ fwd 1, $CA14_{TAG}$ rev 1) and PCR2 (primers $CA14_{TAG}$ fwd 2, $CA14_{ApaI}$ rev 2) were performed in parallel to generate two overlapping single-stranded PCR products. PCR3 with primers $CA14_{BssHII}$ fwd 1 and $CA14_{ApaI}$ rev 2 result in the PCR fragment comprising the mutation, which was subcloned into pNLC4-3* using unique BssHII/ApaI restriction sites, resulting in pNLC4-3*$CA14^{TAG}$ (HIV-1*$CA14^{TAG}$).

Plasmid pNESPlyRS-eRF1dn-tRNA (kindly provided by Anna-Lena Schäfer; Schifferdecker, Sakin et al., in preparation) is based on pEA168 ((Cohen and Arbely 2016); kindly provided by Eyal Arbely, Ben-Gurion University of the Negev, Israel), a eukaryotic vector that comprises expression cassettes for two proteins and four tRNA molecules. The coding sequence for a modified pyrrolysine tRNA synthetase was PCR amplified from plasmid $tRNA^{Pyl}$/$NESPylRS^{AF}$ (Nikić et al. 2016) and cloned into a CMV

bioRxiv preprint doi: https://doi.org/10.1101/2021.09.14.460218; this version posted September 14, 2021. The copyright holder for this preprint (which was not certified by peer review) is the author/funder, who has granted bioRxiv a license to display the preprint in perpetuity. It is made available under aCC-BY 4.0 International license.

promoter driven cassette in pEA168 using HindIII/XbaI restriction sites, resulting in plasmid pEA168-CMV-aaRS-4xU6tRNA. A PCR fragment encoding a dominant version of the eukaryotic release factor 1 (eRF1(E55D)) amplified from plasmid peRF1-E55D (Schmied et al. 2014) was subsequently inserted into an expression cassette driven by the EF1 promotor into pEA168-CMV-aaRS-4xU6tRNA using KpnI/MluI restriction sites, yielding pNESPlyRS-eRF1dn-tRNA.

Cell culture

HEK293T (Pear et al. 1993) and HeLa TZM-bl indicator cells (Wei et al. 2002) were maintained in Dulbecco´s Modified Eagle´s medium (Thermo Fisher Scientific) supplemented with 100 U/ml penicillin, 100 µg/ml streptomycin (PAN Biotech, GER) and 10% fetal calf serum (FCS, Sigma Aldrich, USA). Both cell lines were regularly monitored for mycoplasma contamination using the MycoAlert mycoplasma detection kit (Lonza Rockland, USA). Primary CD4+ T cells were cultured in RPMI 1640 containing L-glutamine supplemented with 100 U/ml penicillin, 100 µg/ml streptomycin (PAN Biotech), 10% heat-inactivated FCS, and 5% human AB serum (Sigma Aldrich).

Isolation of primary cells

Primary human CD4+ T cells were isolated from buffy coats obtained from healthy and anonymous blood donors at the Heidelberg University Hospital Blood Bank following the regulations of the local ethics committee. CD4+ T cells were isolated using EasySep™ Direct Human T Cell Isolation Kit (Stemcell technologies, GER) according to the manufacturer's instructions and activated by incubation in the presence of 100 U/ml IL-2 (Sigma Aldrich) and T Cell TransAct™ human (Miltenyi Biotec, GER) for 72 h.

Virus particle production

HEK293T cells were seeded in T175 tissue culture flasks the day before (~15 Mio. cells) and transfected using calcium phosphate precipitation according to standard procedures (~80 % confluency). Cells were co-transfected with 50 µg / flask total DNA of pNLC4-3* (HIV-1*) or pNLC4-3*CA14^{TAG} (HIV-1*CA14^{TAG}) and plasmid pNESPlyRS-eRF1dn-tRNA in a molar ratio of 2.22:1. At 6 h p.t., medium was removed, and fresh complete DMEM containing a final concentration of 500 µM CpK (SiChem, GER; stock solution 100 mM was pre-diluted 1:4 in 1M HEPES shortly before use),

bioRxiv preprint doi: https://doi.org/10.1101/2021.09.14.460218; this version posted September 14, 2021. The copyright holder for this preprint (which was not certified by peer review) is the author/funder, who has granted bioRxiv a license to display the preprint in perpetuity. It is made available under aCC-BY 4.0 International license.

and 100 µM ascorbic acid (Sigma Aldrich; stock solution 10mM) was added. At 48 h p.t. the tissue culture supernatant was harvested and filtered through 0.45 µm nitrocellulose filters (Carl Roth, GER). For labeling the CA protein, 250 nM Tetrazine-SiR (Spirochrome, GER; stock solution 1 mM) was added to the filtered supernatant, and samples were incubated at 37°C for 30 min. Particles were then concentrated by ultracentrifugation through a 20% (w/v) sucrose cushion at 28,000 rpm using a Beckman TLA-100 fixed angle-rotor (Beckman Coulter, GER) for 90 min at 4°C. Pellets were gently resuspended in phosphate-buffered saline (PBS) containing 10% FCS and 10 mM HEPES (pH 7.5) and stored in 5 µl aliquots at -80°C.

Immunoblotting and In-gel fluorescence

Virus samples were mixed 1:10 with SDS sample buffer (150 mM Tris HCl, pH 6.8, 6% (w/v) SDS, 30% Glycerin, 0.06% bromophenol blue, 20% β -Mercaptoethanol) and boiled at 95°C for 15 min. 10 µl HIV-1* and 40 µl HIV-1*CA^{SiR} lysates were subjected to SDS-PAGE (15 %; acrylamide:bis-acrylamide 200:1). Cell lysates were generated from transfected HEK293T cells. At 40 h p.t. cells were washed with PBS, trypsinized and resuspended in PBS. 1 ml of cell suspension was mixed with 300 µl SDS sample buffer and boiled at 95°C for 15 min. 10 µl cell lysate was subjected to SDS-PAGE. Proteins were transferred to a nitrocellulose membrane (Millipore, USA) by semi-dry blotting for 1 h at 0.8 mA/cm^2. Viral antigens were stained with the indicated antisera in PBS/0.5% bovine serum albumin (BSA) (sheepαCA, polyclonal 1:5,000 (B. Müller et al. 2009); rabbitαMA, polyclonal 1:1,000 (in-house); rabbitαRT, polyclonal, 1:1,000 (B. Müller et al. 2004), mouseαlaminA/C, monoclonal 1:100 (Santa Cruz Biotechnology, GER), mouseαlaminB1, monoclonal 1:100 (Santa Cruz Biotechnology)) followed by staining with corresponding secondary antibodies IRDye™ in PBS/0.5% BSA (anti-sheep 680CW (1;10,000); Rockland, USA and anti-rabbit 800CW (1:10,000); Li-COR Biosciences, GER). Detection was performed using a Li-COR Odyssey CLx infrared scanner (Li-COR Biosciences) according to manufacturer's instructions. CA quantification was performed with ImageStudio LITE software (Li-COR Biosciences) via intensity measurements of CA bands and a serial dilution of recombinant CA standard (2.5 ng/µl; in-house) on the same membrane. For in-gel fluorescence, the acrylamide gels were directly scanned using a Li-COR Odyssey CLx infrared scanner (Li-COR Biosciences) set at an emission wavelength of 700 nm.

bioRxiv preprint doi: https://doi.org/10.1101/2021.09.14.460218; this version posted September 14, 2021. The copyright holder for this preprint (which was not certified by peer review) is the author/funder, who has granted bioRxiv a license to display the preprint in perpetuity. It is made available under aCC-BY 4.0 International license.

Infectivity assay

Virus amounts were quantified via SYBR Green based Product Enhanced Reverse Transcription assay (SG-PERT;(Pizzato et al. 2009)). To determine the effect of incorporating CpK and Tet-SiR labeling on virus infectivity, HIV-1* and HIV-1*CA14^{SiR} viral particles (normalized by RT activity) were titrated on TZM-bl cells seeded in xxx plates. At 6 h p.i. 50 µM T-20 (Enfuvirtide; Roche, GER; stock solution 20 mM) was added to prevent second-round infection. Infection rates were scored at 48 h p.i.. For this, cells were fixed in 4% paraformaldehyde (PFA; Electron Microscopy Sciences, USA; stock solution 16%) for 15 min, followed by 20 min incubation in PBS/0.5% (v/v) Triton X-100 at room temperature. Immunostaining was performed using an in-house polyclonal rabbit antiserum raised against recombinant HIV-1 MA (1:1000) in PBS/0.5% BSA) 1 h at room temperature. Secondary antibody Alexa Fluor 488 donkey anti-rabbit (1:1,000; Thermo Fisher Scientific) in PBS/0.5% BSA was added for 45 min at room temperature. Samples were imaged by SDCM. The mean intensity of the 488 channel (MA(IF)) was quantified in from the non-infected samples imaged in parallel and subtracted as background in each image. The proportion of IF-positive cells was counted in 12 randomly selected fields of view using Fiji (Schindelin et al. 2012). To determine the infectivity of virus particle preparations, the number of infected cells per well was calculated by multiplying the percentage of infected cells detected with the number of cells per well (double of seeded cell number the day before). Division by the volume of virus suspension used for infection yielded the number of infectious units (IU) / ml.

Fixation and immunofluorescence staining of infected cells

3.33×10^3 TZM-bl cells were seeded into 15-well µ-Slides Angiogenesis (ibidi, GER; cat. 81507) the day before infection. Infection at 37°C was performed with an MOI ~0.8 for 6,9,12 or 18 h. Subsequently, cells were incubated for 1 h with 15 µM PF74 (Sigma Aldrich; stock solution 10 mM in DMSO) in DMEM to allow for efficient detection of nuclear CA by IF (T. G. Müller et al. 2021). Samples were washed with PBS, fixed in 4% PFA for 15 min and permeabilized with PBS/0.5% (v/v) Triton-X100 for 20 min, and washed again with PBS. Cells were extracted using ice-cold 100% methanol for 10 min. Afterward, samples were blocked with PBS/2.5% BSA for 15 min, followed by incubation with primary antibodies in PBS/0.5% BSA for 1 h at room temperature. After

bioRxiv preprint doi: https://doi.org/10.1101/2021.09.14.460218; this version posted September 14, 2021. The copyright holder for this preprint (which was not certified by peer review) is the author/funder, who has granted bioRxiv a license to display the preprint in perpetuity. It is made available under aCC-BY 4.0 International license.

washing three times with PBS, secondary antibodies diluted in PBS/0.5% BSA were added for 45 min at room temperature. Samples were washed and stored in PBS at 4°C. For infection of primary $CD4^+$ T cells, 20,000 cells were infected with HIV-1* or HIV-1*$CA14^{SiR}$ in a 96-well v-bottom microplate (Greiner Bio-one, GER; cat. 650161) in a volume of 40 µl RPMI and transferred at 22 h p.i. onto a PEI-coated 15-well µ-Slide Angiogenesis (ibidi). Cells were allowed to adhere for 1 h at 37°C, and PF74 diluted in fresh growth medium was added to a final concentration of 15 µM. Extraction, fixation, and immunostaining were performed after 1 h at 37°C as described above. For the detection of endosome-associated particles, 2 µM mCLING ATTO488 (Synaptic Systems, GER; stock 50 µM) was added to TZM-bl cells seeded in 15-well µ-Slides Angiogenesis and incubated at 16°C for 30 min. Subsequently, the fluorescent probe was removed, HIV-1*$CA14^{SiR}$ particles were added in fresh growth medium, and cells were incubated for an additional 3 h at 37°C (MOI~0.8). Cells were fixed for 90 min at room temperature in 4% PFA and 0.2% glutaraldehyde to ensure retention of mCLING at cellular membranes. Nuclei were stained with 5 µg/ml Hoechst (Merck) in PBS for 30 min.

Cell viability assay

To test the effect of mCLING ATTO488 (Synaptic Systems) staining on cell viability, TZM-bl cells were seeded into a 96-well plate ($9x10^3$ cells/well; flat bottom Greiner Bio-one, DE) the day before and incubated in medium supplemented with the indicated concentration of mCLING ATTO488 for 30 min at 16°C. After staining, cells were trypsinized and stained with Trypan blue (Strober 2001) using standard procedures and analyzed with a TC20™ Automated Cell Counter (BioRad, GER).

Labelling efficiency of immobilized particles

15-well µ-Slide Angiogenesis (ibidi) were coated with 30µl/well polyethyleneimine (PEI; 1mg/ml) for 30 min at room temperature and washed with PBS. Pre-labeled HIV-1* and HIV-1*$CA14^{SiR}$ particles were incubated in PBS on PEI-coated microscopy slides for 1 h at 37°C. Subsequently, samples were washed with PBS, fixed in 4% PFA for 15 min and permeabilized with PBS/0.05% (v/v) Triton X-100 for 20 min at room temperature. Immobilized particles were blocked with PBS/2.5% BSA for 15 min and polyclonal rabbit antiserum raised against recombinant HIV-1 CA protein (in-house) was added (1:1000 in PBS/0.5% BSA for 1 h at room temperature). After washing three

bioRxiv preprint doi: https://doi.org/10.1101/2021.09.14.460218; this version posted September 14, 2021. The copyright holder for this preprint (which was not certified by peer review) is the author/funder, who has granted bioRxiv a license to display the preprint in perpetuity. It is made available under aCC-BY 4.0 International license.

times with PBS, secondary antibody Alexa Fluor 488 donkey anti-rabbit (Thermo Fisher Scientific) 1:1000 in PBS/0.5% BSA was added for 45 min at room temperature. Samples were washed and stored in PBS at 4°C.

Confocal microscopy (SDCM)

Multichannel z-series with a z-spacing of 200 nm, spanning the whole cell volume (3D), were acquired using a PerkinElmer Ultra VIEW VoX 3D spinning disk confocal microscope (SDCM; Perkin Elmer, MA, USA). A 60x oil immersion objective (numeric aperture [NA] 1.49; Perkin Elmer) was used for imaging of TZM-bl cells or 100x oil immersion objective ([NA] 1.49; Perkin Elmer) for primary CD4+ T cells and immobilized particles. Images were recorded in the 405-, 488-, 561-, and 640 nm channels.

STED microscopy

STED nanoscopy was performed using a λ = 775 nm STED system (Abberior Instruments GmbH, GER) equipped with a 100x oil immersion objective (NA 1.4; Olympus UPlanSApo). STED images were acquired using the 640 nm excitation laser lines while the 488 and 590 laser line was acquired in confocal mode only. Nominal STED laser power was set to 20% of the maximal power (1250 mW) with pixel dwell time of 10 µs and 15 nm pixel size. STED images were deconvolved using the software Imspector (Abberior Instruments GmbH) and Huygens Professional Deconvolution (Scientific Volume Imaging, NED).

Electron microscopy

HEK293T cells (4×10^5) were seeded in a glass coverslip-bottom petri dish (MatTek, MA, USA), cultured for 16 h at 37°C and then co-transfected with pNLC4-3*CA14^{TAG} and pNESPlyRS-eRF1dn-tRNA by using calcium phosphate precipitation. At 6 h p.t., medium was removed and fresh complete DMEM containing a final concentration of 500 µM CpK (SiChem, GER; stock solution 100 mM was pre-diluted 1:4 in 1M HEPES shortly before use), and 100 µM ascorbic acid (Sigma Aldrich; stock solution 10mM) was added. At 44 h p.t., cells were fixed with pre-warmed 2% formaldehyde + 2.5% glutaraldehyde in 0.1M cacodylate buffer (pH 7.4) for 1.5 h at room temperature, then washed in 0.1M cacodylate buffer and post-fixed with 2% osmium tetroxide (Electron Microscopy Sciences) for a 1 h on ice. Cells were subsequently dehydrated through

bioRxiv preprint doi: https://doi.org/10.1101/2021.09.14.460218; this version posted September 14, 2021. The copyright holder for this preprint (which was not certified by peer review) is the author/funder, who has granted bioRxiv a license to display the preprint in perpetuity. It is made available under aCC-BY 4.0 International license.

an increasing cold ethanol series (30, 50, 70, 80, 90, and 100%; on ice) and two anhydrous acetone series (at room temperature). The coverslip with cells was then removed from the dish, and cells were flat embedded in Epon resin. 70-nm thin sections were cut with an ultramicrotome (Leica EM UC6), collected on formvar-coated 100-mesh copper EM grids (Electron Microscopy Sciences) and stained with a 3% uranyl acetate in 70% MetOH (10 min), and lead citrate (7 min). Cells sections were observed with a JEOL JEM-1400 electron microscope operating at 80 kV (Jeol Ltd., JPN), equipped with a bottom-mounted 4K by 4K pixel digital camera (TemCam F416; TVIPS GmbH, GER).

CLEM and electron tomography

SupT1 cells were distributed in a 96-well plate ($2x10^5$ cells/well; U-bottom; Greiner Bio-one, 650180) and pre-incubated for 16 h with 1µm aphidicolin (APC; Merck). Cells were pelleted (200 x g, 3 min) and resuspended in complete RPMI medium containing HIV-1*CA14^{SIR} particles (MOI~0.4). Cells were incubated with viral particles for 120 min at 16°C to adsorb the virus and synchronize virus entry. Samples were then processed for CLEM and ET as described previously (Zila et al. 2021). In brief, cells were transferred to glass-bottomed 'microwell' of MatTek dish (MatTek, USA) containing carbon-coated and retronectin-coated sapphire discs (Engineering Office M. Wohlwend, SUI). Samples were high pressure frozen, and sapphire discs were then transferred from liquid nitrogen to the freeze-substitution (FS) medium (0.1% uranyl acetate, 2.3% methanol and 2% H_2O in acetone) tempered at -90°C. Samples were FS-processed and embedded in Lowicryl HM20 resin (Polysciences, USA) according to a modified protocol of Kukulski et al. (Kukulski et al. 2011). For CLEM-ET, thick resin sections (250 nm) were cut and placed on a slot (1 × 2 mm) EM copper grids covered with a formvar film (Electron Microscopy Sciences, FF2010-Cu). Grids were decorated with fiducial marker and stained with Hoechst to visualize nuclear regions. Light microscopy Z stacks of sections were acquired by PerkinElmer UltraVIEW VoX 3D Spinning-disc Confocal Microscope (Perkin Elmer) using a 100 × oil immersion objective (NA 1.49; Nikon), with a *z*-spacing of 200 nm and excitation with the 405-, 488-, 561- and 633-nm laser line. Acquired z stacks were visually examined using Fiji software (Schindelin et al. 2012) and intracellular CA(SiR) positive signals were identified. EM grids were decorated with 15 nm protein-A gold particles for tomogram alignment and stained with uranyl acetate and lead citrate. Grids were loaded to a

bioRxiv preprint doi: https://doi.org/10.1101/2021.09.14.460218; this version posted September 14, 2021. The copyright holder for this preprint (which was not certified by peer review) is the author/funder, who has granted bioRxiv a license to display the preprint in perpetuity. It is made available under aCC-BY 4.0 International license.

Tecnai TF20 (FEI) electron microscope (operated at 200 kV) equipped with a field emission gun and a 4K by 4K pixel Eagle CCD camera (FEI). Positions of CA(SiR) signals were pre-correlated with imported SDCM images in SerialEM (Mastronarde 2005) as described previously (Schorb et al. 2017). Single-axis electron tomograms were carried out. Tomographic tilt ranges were typically from –60° to 60° with an angular increment of 1°. The pixel size was 1.13 nm. Alignments and 3D reconstructions of tomograms were done with IMOD software (Kremer, Mastronarde, and McIntosh 1996). Post-correlation was performed using eC-CLEM plugin (Paul-Gilloteaux et al. 2017) in Icy software (De Chaumont et al. 2012).

Image analysis

Microscopy images were screened and filtered in Fiji/ImageJ (Schindelin et al. 2012) with a mean filter and background subtraction. Infected cells were quantified in Fiji via segmentation and counting of nuclei and the cell counter to manually quantify the number of positive cells.

To determine labeling efficiency of click labeled particles, CA(SiR) intensities of detected immobilized particles based on CA(IF) were quantified using the spot detector of the software Icy (De Chaumont et al. 2012). 5 ROIs without particles were measured and mean intensity in the SiR channel was subtracted as background. Threshold was set to t = 1,000 a.u.. Every CA(IF) detected spot above was considered CA(SiR) positive.

To analyze particle distribution and intensity measurements throughout the entire volume of cells, z-image series were reconstructed in 3D space using Imaris 9.2 software (Bitplane AG, SUI). Individual HIV-1 CA(IF) objects were automatically detected using the spot detector Imaris module, which created for each fluorescent signal a 3D ellipsoid object with 300 nm estimated diameter in *x-y* dimensions and 600 nm in *z*. The local background of each individual spot was subtracted automatically. Subsequently, the mean signal intensity in the CA(SiR) channel was quantitated within all objects. The threshold for SiR intensity was set to t = 7,000 a.u. and adjusted manually for each image by visual inspection. Spots detected in SiR-clusters were excluded. Nuclear objects were manually identified based on the laminA/C staining. NE-associated objects were classified based on laminA/C intensities. Every image was manually inspected and a threshold for NE-associated objects was set in the range of

bioRxiv preprint doi: https://doi.org/10.1101/2021.09.14.460218; this version posted September 14, 2021. The copyright holder for this preprint (which was not certified by peer review) is the author/funder, who has granted bioRxiv a license to display the preprint in perpetuity. It is made available under aCC-BY 4.0 International license.

6,300-9,100 a.u.. All other particles were classified as PM/cytoplasm (= in the cytoplasm/at plasma membrane).

To identify post-fusion cores by mCLING ATTO488 staining, HIV-1 CA(SiR) positive objects were automatically detected and the mCLING ATTO488 mean signal intensity co-localizing with each object was quantitated. The threshold was set to t = 5,900 a.u. based on the lowest mCLING intensity detected in a T-20 control sample. Particles associated with mCLING intensity above background were classified as endosome associated. Fiji standard 'greyscale' lookup table (LUT) was used to visualize single channel images and 'Fire' for single channel STED images.

Data visualization and statistical analysis

Statistical significance was assessed using Prism v9.1.0 (GraphPad Software Inc, USA). A two-tailed non-paired Mann-Whitney test (α = 0.05) was used to assess the statistical significance of non-parametric data. Data were plotted using Prism v9.1.0 or the Python statistical data visualization package seaborn v.0.10.0 (Waskom et al., 2020). Graphs show mean/median with error bars as defined in the figure legends.

Competing financial interests: The authors declare no competing financial interests.

References

Adachi, A, H E Gendelman, S Koenig, T Folks, R Willey, A Rabson, and M A Martin. 1986. "Production of Acquired Immunodeficiency Syndrome-Associated Retrovirus in Human and Nonhuman Cells Transfected with an Infectious Molecular Clone." *Journal of Virology* 59 (2): 284–91. https://doi.org/10.1128/jvi.59.2.284-291.1986.

Arhel, Nathalie J., Sylvie Souquere-Besse, Sandie Munier, Philippe Souque, Stéphanie Guadagnini, Sandra Rutherford, Marie Christine Prévost, Terry D. Allen, and Pierre Charneau. 2007. "HIV-1 DNA Flap Formation Promotes Uncoating of the Pre-Integration Complex at the Nuclear Pore." *EMBO Journal* 26 (12): 3025–37. https://doi.org/10.1038/sj.emboj.7601740.

Asokan, Aravind, David V. Schaffer, and R. Jude Samulski. 2012. "The AAV Vector Toolkit: Poised at the Clinical Crossroads." *Molecular Therapy* 20 (4): 699–708. https://doi.org/10.1038/mt.2011.287.

bioRxiv preprint doi: https://doi.org/10.1101/2021.09.14.460218; this version posted September 14, 2021. The copyright holder for this preprint (which was not certified by peer review) is the author/funder, who has granted bioRxiv a license to display the preprint in perpetuity. It is made available under aCC-BY 4.0 International license.

Balzarotti, Francisco, Yvan Eilers, Klaus C Gwosch, Arvid H Gynnå, Volker Westphal, Fernando D Stefani, Johan Elf, and Stefan W Hell. 2017. "With Minimal Photon Fluxes." *Science* 355 (February): 606–12. https://doi.org/10.1126/science.aak9913.

Bhattacharya, Akash, Steven L. Alam, Thomas Fricke, Kaneil Zadrozny, Jaroslaw Sedzicki, Alexander B. Taylor, Borries Demeler, et al. 2014. "Structural Basis of HIV-1 Capsid Recognition by PF74 and CPSF6." *Proceedings of the National Academy of Sciences* 111 (52): 18625–30. https://doi.org/10.1073/pnas.1419945112.

Blair, Wade S., Chris Pickford, Stephen L. Irving, David G. Brown, Marie Anderson, Richard Bazin, Joan Cao, et al. 2010. "HIV Capsid Is a Tractable Target for Small Molecule Therapeutic Intervention." *PLoS Pathogens* 6 (12). https://doi.org/10.1371/journal.ppat.1001220.

Blanco-Rodriguez, Guillermo, Anastasia Gazi, Blandine Monel, Stella Frabetti, Viviana Scoca, Florian Mueller, Olivier Schwartz, Jacomine Krijnse-Locker, Pierre Charneau, and Francesca Di Nunzio. 2020. "Remodeling of the Core Leads HIV-1 Preintegration Complex into the Nucleus of Human Lymphocytes." *Journal of Virology* 94 (11). https://doi.org/10.1128/jvi.00135-20.

Bohne, Jens, and Hans Georg Kräusslich. 2004. "Mutation of the Major 5′ Splice Site Renders a CMV-Driven HIV-1 Proviral Clone Tat-Dependent: Connections between Transcription and Splicing." *FEBS Letters* 563 (1–3): 113–18. https://doi.org/10.1016/S0014-5793(04)00277-7.

Börner, Kathleen, Eike Kienle, Lin Ya Huang, Jonas Weinmann, Anna Sacher, Philipp Bayer, Christian Stüllein, et al. 2020. "Pre-Arrayed Pan-AAV Peptide Display Libraries for Rapid Single-Round Screening." *Molecular Therapy* 28 (4): 1016–32. https://doi.org/10.1016/j.ymthe.2020.02.009.

Briggs, J. A G, Martha N. Simon, Ingolf Gross, Hans Georg Kräusslich, Stephen D. Fuller, Volker M. Vogt, and Marc C. Johnson. 2004. "The Stoichiometry of Gag Protein in HIV-1." *Nature Structural and Molecular Biology* 11 (7): 672–75. https://doi.org/10.1038/nsmb785.

Briggs, John A.G., Thomas Wilk, Reinhold Welker, Hans Georg Kräusslich, and Stephen D. Fuller. 2003. "Structural Organization of Authentic, Mature HIV-1

bioRxiv preprint doi: https://doi.org/10.1101/2021.09.14.460218; this version posted September 14, 2021. The copyright holder for this preprint (which was not certified by peer review) is the author/funder, who has granted bioRxiv a license to display the preprint in perpetuity. It is made available under aCC-BY 4.0 International license.

Virions and Cores." *EMBO Journal* 22 (7): 1707–15. https://doi.org/10.1093/emboj/cdg143.

Bukrinsky, Michael I., Sheryl Haggerty, Michael P. Dempsey, Natalia Sharova, Alexei Adzhubei, Lynn Spitz, Paul Lewis, David Goldfarb, Michael Emerman, and Mario Stevenson. 1993. "A Nuclear Localization Signal within HIV-1 Matrix Protein That Governs Infection of Non-Dividing Cells." *Nature* 365 (6447): 666–69. https://doi.org/10.1038/365666a0.

Burdick, Ryan C., Krista A. Delviks-Frankenberry, Jianbo Chen, Sanath K. Janaka, Jaya Sastri, Wei Shau Hu, and Vinay K. Pathak. 2017. *Dynamics and Regulation of Nuclear Import and Nuclear Movements of HIV-1 Complexes*. *PLoS Pathogens*. Vol. 13. https://doi.org/10.1371/journal.ppat.1006570.

Burdick, Ryan C., Chenglei Li, Mohamed Husen Munshi, Jonathan M.O. Rawson, Kunio Nagashima, Wei Shau Hu, and Vinay K. Pathak. 2020. "HIV-1 Uncoats in the Nucleus near Sites of Integration." *Proceedings of the National Academy of Sciences of the United States of America* 117 (10): 5486–93. https://doi.org/10.1073/pnas.1920631117.

Campbell, Edward M., and Thomas J. Hope. 2015. "HIV-1 Capsid: The Multifaceted Key Player in HIV-1 Infection." *Nature Reviews Microbiology* 13 (8): 471–83. https://doi.org/10.1038/nrmicro3503.

Campbell, Edward M., Omar Perez, Jenny L. Anderson, and Thomas J. Hope. 2008. "Visualization of a Proteasome-Independent Intermediate during Restriction of HIV-1 by Rhesus TRIM5α." *Journal of Cell Biology* 180 (3): 549–61. https://doi.org/10.1083/jcb.200706154.

Carlson, Lars Anders, John A.G. Briggs, Bärbel Glass, James D. Riches, Martha N. Simon, Marc C. Johnson, Barbara Müller, Kay Grünewald, and Hans Georg Kräusslich. 2008. "Three-Dimensional Analysis of Budding Sites and Released Virus Suggests a Revised Model for HIV-1 Morphogenesis." *Cell Host and Microbe* 4 (6): 592–99. https://doi.org/10.1016/j.chom.2008.10.013.

Chaumont, Fabrice De, Stéphane Dallongeville, Nicolas Chenouard, Nicolas Hervé, Sorin Pop, Thomas Provoost, Vannary Meas-Yedid, et al. 2012. "Icy: An Open Bioimage Informatics Platform for Extended Reproducible Research." *Nature Methods* 9 (7): 690–96. https://doi.org/10.1038/nmeth.2075.

bioRxiv preprint doi: https://doi.org/10.1101/2021.09.14.460218; this version posted September 14, 2021. The copyright holder for this preprint (which was not certified by peer review) is the author/funder, who has granted bioRxiv a license to display the preprint in perpetuity. It is made available under aCC-BY 4.0 International license.

Chen, Nan Yu, Lihong Zhou, Paul J. Gane, Silvana Opp, Neil J. Ball, Giuseppe Nicastro, Madeleine Zufferey, et al. 2016. "HIV-1 Capsid Is Involved in Post-Nuclear Entry Steps." *Retrovirology* 13 (1): 1–16. https://doi.org/10.1186/s12977-016-0262-0.

Cohen, Sarit, and Eyal Arbely. 2016. "Single-Plasmid-Based System for Efficient Noncanonical Amino Acid Mutagenesis in Cultured Mammalian Cells." *ChemBioChem* 17 (11): 1008–11. https://doi.org/10.1002/cbic.201500681.

Cosnefroy, Ophélie, Philip J. Murray, and Kate N. Bishop. 2016. "HIV-1 Capsid Uncoating Initiates after the First Strand Transfer of Reverse Transcription." *Retrovirology* 13 (1): 1–17. https://doi.org/10.1186/s12977-016-0292-7.

Dharan, Adarsh, Niklas Bachmann, Sarah Talley, Virginia Zwikelmaier, and Edward M. Campbell. 2020. "Nuclear Pore Blockade Reveals That HIV-1 Completes Reverse Transcription and Uncoating in the Nucleus." *Nature Microbiology* 5 (9): 1088–95. https://doi.org/10.1038/s41564-020-0735-8.

Engelman, Alan N. 2021. "Hiv Capsid and Integration Targeting." *Viruses* 13 (1): 1–14. https://doi.org/10.3390/v13010125.

Erdmann, Roman S., Hideo Takakura, Alexander D. Thompson, Felix Rivera-Molina, Edward S. Allgeyer, Joerg Bewersdorf, Derek Toomre, and Alanna Schepartz. 2014. "Super-Resolution Imaging of the Golgi in Live Cells with a Bioorthogonal Ceramide Probe." *Angewandte Chemie - International Edition* 53 (38): 10242–46. https://doi.org/10.1002/anie.201403349.

Fassati, Ariberto. 2012. "Multiple Roles of the Capsid Protein in the Early Steps of HIV-1 Infection." *Virus Research* 170 (1–2): 15–24. https://doi.org/10.1016/j.virusres.2012.09.012.

Fassati, Ariberto, and Sp Goff. 2001. "Characterization of Intracellular Reverse Transcription Complexes of Human Immunodeficiency Virus Type 1." *Journal of Virology* 75 (8): 3626–35. https://doi.org/10.1128/JVI.75.8.3626.

Fernandez, Juliette, Anthony K. Machado, Sébastien Lyonnais, Célia Chamontin, Kathleen Gärtner, Thibaut Léger, Corinne Henriquet, et al. 2019. "Transportin-1 Binds to the HIV-1 Capsid via a Nuclear Localization Signal and Triggers Uncoating." *Nature Microbiology* 4 (11): 1840–50. https://doi.org/10.1038/s41564-019-0575-6.

bioRxiv preprint doi: https://doi.org/10.1101/2021.09.14.460218; this version posted September 14, 2021. The copyright holder for this preprint (which was not certified by peer review) is the author/funder, who has granted bioRxiv a license to display the preprint in perpetuity. It is made available under aCC-BY 4.0 International license.

Francis, Ashwanth C., Mariana Marin, Mathew J. Prellberg, Kristina Palermino-Rowland, and Gregory B. Melikyan. 2020. "Hiv-1 Uncoating and Nuclear Import Precede the Completion of Reverse Transcription in Cell Lines and in Primary Macrophages." *Viruses* 12 (11): 1–22. https://doi.org/10.3390/v12111234.

Francis, Ashwanth C., Mariana Marin, Jiong Shi, Christopher Aiken, and Gregory B. Melikyan. 2016. "Time-Resolved Imaging of Single HIV-1 Uncoating In Vitro and in Living Cells." *PLoS Pathogens* 12 (6): 1–28. https://doi.org/10.1371/journal.ppat.1005709.

Francis, Ashwanth C., Mariana Marin, Parmit K. Singh, Vasudevan Achuthan, Mathew J. Prellberg, Kristina Palermino-Rowland, Shuiyun Lan, et al. 2020. "HIV-1 Replication Complexes Accumulate in Nuclear Speckles and Integrate into Speckle-Associated Genomic Domains." *Nature Communications* 11 (1). https://doi.org/10.1038/s41467-020-17256-8.

Francis, Ashwanth C., and Gregory B. Melikyan. 2018. "Single HIV-1 Imaging Reveals Progression of Infection through CA-Dependent Steps of Docking at the Nuclear Pore, Uncoating, and Nuclear Transport." *Cell Host and Microbe* 23 (4): 536-548.e6. https://doi.org/10.1016/j.chom.2018.03.009.

Ganser-Pornillos, Barbie K., Anchi Cheng, and Mark Yeager. 2007. "Structure of Full-Length HIV-1 CA: A Model for the Mature Capsid Lattice." *Cell* 131 (1): 70–79. https://doi.org/10.1016/j.cell.2007.08.018.

Golding, Hana, Marina Zaitseva, Eve de Rosny, Lisa R. King, Jody Manischewitz, Igor Sidorov, Miroslaw K. Gorny, Susan Zolla-Pazner, Dimiter S. Dimitrov, and Carol D. Weiss. 2002. "Dissection of Human Immunodeficiency Virus Type 1 Entry with Neutralizing Antibodies to Gp41 Fusion Intermediates." *Journal of Virology* 76 (13): 6780–90. https://doi.org/10.1128/jvi.76.13.6780-6790.2002.

Grime, John M.A., and Gregory A. Voth. 2012. "Early Stages of the HIV-1 Capsid Protein Lattice Formation." *Biophysical Journal* 103 (8): 1774–83. https://doi.org/10.1016/j.bpj.2012.09.007.

Grimm, Dirk, and Sergei Zolotukhin. 2015. "E Pluribus Unum: 50 Years of Research, Millions of Viruses, and One Goal-Tailored Acceleration of AAV Evolution." *Molecular Therapy* 23 (12): 1819–31. https://doi.org/10.1038/mt.2015.173.

Guedán, Anabel, Eve R Caroe, Genevieve C R Barr, and Kate N Bishop. 2021. "The

bioRxiv preprint doi: https://doi.org/10.1101/2021.09.14.460218; this version posted September 14, 2021. The copyright holder for this preprint (which was not certified by peer review) is the author/funder, who has granted bioRxiv a license to display the preprint in perpetuity. It is made available under aCC-BY 4.0 International license.

Role of Capsid in HIV-1 Nuclear Entry," 1–14.

Heilemann, Mike, Sebastian Van De Linde, Mark Schüttpelz, Robert Kasper, Britta Seefeldt, Anindita Mukherjee, Philip Tinnefeld, and Markus Sauer. 2008. "Subdiffraction-Resolution Fluorescence Imaging with Conventional Fluorescent Probes." *Angewandte Chemie - International Edition* 47 (33): 6172–76. https://doi.org/10.1002/anie.200802376.

Hulme, Amy E., and Thomas J. Hope. 2014. "The Cyclosporin A Washout Assay to Detect HIV-1 Uncoating in Infected Cells." In , 37–46. https://doi.org/10.1007/978-1-62703-670-2_4.

Hulme, Amy E., Omar Perez, and Thomas J. Hope. 2011. "Complementary Assays Reveal a Relationship between HIV-1 Uncoating and Reverse Transcription." *Proceedings of the National Academy of Sciences of the United States of America* 108 (24): 9975–80. https://doi.org/10.1073/pnas.1014522108.

Kane, Melissa, Stephanie V. Rebensburg, Matthew A. Takata, Trinity M. Zang, Masahiro Yamashita, Mamuka Kvaratskhelia, and Paul D. Bieniasz. 2018. "Nuclear Pore Heterogeneity Influences HIV-1 Infection and the Antiviral Activity of MX2." *ELife* 7: 1–44. https://doi.org/10.7554/eLife.35738.

Katrekar, Dhruva, Ana M. Moreno, Genghao Chen, Atharv Worlikar, and Prashant Mali. 2018. "Oligonucleotide Conjugated Multi-Functional Adeno-Associated Viruses." *Scientific Reports* 8 (1): 1–8. https://doi.org/10.1038/s41598-018-21742-x.

Kelemen, Rachel E., Sarah B. Erickson, and Abhishek Chatterjee. 2018. "Synthesis at the Interface of Virology and Genetic Code Expansion." *Current Opinion in Chemical Biology* 46: 164–71. https://doi.org/10.1016/j.cbpa.2018.07.015.

Klar, Thomas A., and Stefan W. Hell. 1999. "Subdiffraction Resolution in Far-Field Fluorescence Microscopy." *Optics Letters* 24 (14): 954. https://doi.org/10.1364/OL.24.000954.

Knockenhauer, Kevin E., and Thomas U. Schwartz. 2016. "The Nuclear Pore Complex as a Flexible and Dynamic Gate." *Cell* 164 (6): 1162–71. https://doi.org/10.1016/j.cell.2016.01.034.

Kotterman, Melissa A., and David V. Schaffer. 2014. "Engineering Adeno-Associated Viruses for Clinical Gene Therapy." *Nature Reviews Genetics* 15 (7): 445–51.

bioRxiv preprint doi: https://doi.org/10.1101/2021.09.14.460218; this version posted September 14, 2021. The copyright holder for this preprint (which was not certified by peer review) is the author/funder, who has granted bioRxiv a license to display the preprint in perpetuity. It is made available under aCC-BY 4.0 International license.

https://doi.org/10.1038/nrg3742.

Krauskopf, Kristina, and Kathrin Lang. 2020. "Increasing the Chemical Space of Proteins in Living Cells via Genetic Code Expansion." *Current Opinion in Chemical Biology* 58: 112–20. https://doi.org/10.1016/j.cbpa.2020.07.012.

Kremer, James R., David N. Mastronarde, and J. Richard McIntosh. 1996. "Computer Visualization of Three-Dimensional Image Data Using IMOD." *Journal of Structural Biology* 116 (1): 71–76. https://doi.org/10.1006/jsbi.1996.0013.

Kukulski, Wanda, Martin Schorb, Sonja Welsch, Andrea Picco, Marko Kaksonen, and John A.G. Briggs. 2011. "Correlated Fluorescence and 3D Electron Microscopy with High Sensitivity and Spatial Precision." *Journal of Cell Biology* 192 (1): 111–19. https://doi.org/10.1083/jcb.201009037.

la Torre, Daniel de, and Jason W. Chin. 2021. "Reprogramming the Genetic Code." *Nature Reviews Genetics* 22 (3): 169–84. https://doi.org/10.1038/s41576-020-00307-7.

Lang, Kathrin, and Jason W. Chin. 2014. "Bioorthogonal Reactions for Labeling Proteins." *ACS Chemical Biology* 9 (1): 16–20. https://doi.org/10.1021/cb4009292.

Lanman, Jason, Tu Kiet T. Lam, Mark R. Emmett, Alan G. Marshall, Michael Sakalian, and Peter E. Prevelige. 2004. "Key Interactions in HIV-1 Maturation Identified by Hydrogen-Deuterium Exchange." *Nature Structural and Molecular Biology* 11 (7): 676–77. https://doi.org/10.1038/nsmb790.

Lee, K., A. Mulky, W. Yuen, T. D. Martin, N. R. Meyerson, L. Choi, H. Yu, S. L. Sawyer, and V. N. KewalRamani. 2012. "HIV-1 Capsid-Targeting Domain of Cleavage and Polyadenylation Specificity Factor 6." *Journal of Virology* 86 (7): 3851–60. https://doi.org/10.1128/jvi.06607-11.

Lelek, Mickaël, Nicoletta Casartelli, Danilo Pellin, Ermanno Rizzi, Philippe Souque, Marco Severgnini, Clelia Di Serio, et al. 2015. "Chromatin Organization at the Nuclear Pore Favours HIV Replication." *Nature Communications* 6. https://doi.org/10.1038/ncomms7483.

Li, Chenglei, Ryan C. Burdick, Kunio Nagashima, Wei-Shau Hu, and Vinay K. Pathak. 2021. "HIV-1 Cores Retain Their Integrity until Minutes before Uncoating in the Nucleus." *Proceedings of the National Academy of Sciences* 118 (10):

bioRxiv preprint doi: https://doi.org/10.1101/2021.09.14.460218; this version posted September 14, 2021. The copyright holder for this preprint (which was not certified by peer review) is the author/funder, who has granted bioRxiv a license to display the preprint in perpetuity. It is made available under aCC-BY 4.0 International license.

e2019467118. https://doi.org/10.1073/pnas.2019467118.

Liu, Huanting, and James H. Naismith. 2008. "An Efficient One-Step Site-Directed Deletion, Insertion, Single and Multiple-Site Plasmid Mutagenesis Protocol." *BMC Biotechnology* 8: 91. https://doi.org/10.1186/1472-6750-8-91.

Lukic, Zana, Adarsh Dharan, Thomas Fricke, Felipe Diaz-Griffero, and Edward M. Campbell. 2014. "HIV-1 Uncoating Is Facilitated by Dynein and Kinesin 1." *Journal of Virology* 88 (23): 13613–25. https://doi.org/10.1128/jvi.02219-14.

Lukinavičius, Gražvydas, Keitaro Umezawa, Nicolas Olivier, Alf Honigmann, Guoying Yang, Tilman Plass, Veronika Mueller, et al. 2013. "A Near-Infrared Fluorophore for Live-Cell Super-Resolution Microscopy of Cellular Proteins." *Nature Chemistry* 5 (2): 132–39. https://doi.org/10.1038/nchem.1546.

Ma, Yingxin, Zhike He, Tianwei Tan, Wei Li, Zhiping Zhang, Shuang Song, Xiaowei Zhang, et al. 2016. "Real-Time Imaging of Single HIV-1 Disassembly with Multicolor Viral Particles." *ACS Nano* 10 (6): 6273–82. https://doi.org/10.1021/acsnano.6b02462.

Mamede, João I., Gianguido C. Cianci, Meegan R. Anderson, and Thomas J. Hope. 2017. "Early Cytoplasmic Uncoating Is Associated with Infectivity of HIV-1." *Proceedings of the National Academy of Sciences of the United States of America* 114 (34): E7169–78. https://doi.org/10.1073/pnas.1706245114.

Márquez, Chantal L, Derrick Lau, James Walsh, Vaibhav Shah, Conall McGuinness, Andrew Wong, Anupriya Aggarwal, et al. 2018. "Kinetics of HIV-1 Capsid Uncoating Revealed by Single-Molecule Analysis." *ELife* 7: e34772. https://doi.org/10.7554/eLife.34772.

Marsh, Mark, and Ari Helenius. 2006. "Virus Entry: Open Sesame." *Cell* 124 (4): 729–40. https://doi.org/10.1016/j.cell.2006.02.007.

Mastronarde, David N. 2005. "Automated Electron Microscope Tomography Using Robust Prediction of Specimen Movements." *Journal of Structural Biology* 152 (1): 36–51. https://doi.org/10.1016/j.jsb.2005.07.007.

Matreyek, Kenneth A., Sara S. Yücel, Xiang Li, and Alan Engelman. 2013. "Nucleoporin NUP153 Phenylalanine-Glycine Motifs Engage a Common Binding Pocket within the HIV-1 Capsid Protein to Mediate Lentiviral Infectivity." *PLoS Pathogens* 9 (10). https://doi.org/10.1371/journal.ppat.1003693.

bioRxiv preprint doi: https://doi.org/10.1101/2021.09.14.460218; this version posted September 14, 2021. The copyright holder for this preprint (which was not certified by peer review) is the author/funder, who has granted bioRxiv a license to display the preprint in perpetuity. It is made available under aCC-BY 4.0 International license.

Mattei, Simone, Bärbel Glass, Wim J.H. Hagen, Hans Georg Kräusslich, and John A.G. Briggs. 2016. "The Structure and Flexibility of Conical HIV-1 Capsids Determined within Intact Virions." *Science* 354 (6318): 1434–37. https://doi.org/10.1126/science.aah4972.

McArthur, Carole, Fabio Gallazzi, Thomas P. Quinn, and Kamal Singh. 2019. "HIV Capsid Inhibitors Beyond PF74." *Diseases* 7 (4): 56. https://doi.org/10.3390/diseases7040056.

Melikyan, Gregory B. 2014. "HIV Entry: A Game of Hide-and-Fuse?" *Current Opinion in Virology* 4 (2): 1–7. https://doi.org/10.1016/j.coviro.2013.09.004.

Melikyan, Grigory B., Ruben M. Markosyan, Hila Hemmati, Mary K. Delmedico, Dennis M. Lambert, and Fredric S. Cohen. 2000. "Evidence That the Transition of HIV-1 Gp41 into a Six-Helix Bundle, Not the Bundle Configuration, Induces Membrane Fusion." *Journal of Cell Biology* 151 (2): 413–23. https://doi.org/10.1083/jcb.151.2.413.

Miller, M D, C M Farnet, and F D Bushman. 1997. "Human Immunodeficiency Virus Type 1 Preintegration Complexes: Studies of Organization and Composition." *Journal of Virology* 71 (7): 5382–90. https://doi.org/10.1128/jvi.71.7.5382-5390.1997.

Müller, Barbara, Maria Anders, Hisashi Akiyama, Sonja Welsch, Bärbel Glass, Krisztina Nikovics, Francois Clavel, Hanna Mari Tervo, Oliver T. Keppler, and Hans Georg Kräusslich. 2009. "HIV-1 Gag Processing Intermediates Trans-Dominantly Interfere with HIV-1 Infectivity." *Journal of Biological Chemistry* 284 (43): 29692–703. https://doi.org/10.1074/jbc.M109.027144.

Müller, Barbara, Jessica Daecke, Oliver T. Fackler, Matthias T. Dittmar, Hanswalter Zentgraf, and Hans-Georg Kräusslich. 2004. "Construction and Characterization of a Fluorescently Labeled Infectious Human Immunodeficiency Virus Type 1 Derivative." *Journal of Virology* 78 (19): 10803–13. https://doi.org/10.1128/jvi.78.19.10803-10813.2004.

Müller, Barbara, Uwe Tessmer, Ulrich Schubert, and Hans-Georg Kräusslich. 2000. "Human Immunodeficiency Virus Type 1 Vpr Protein Is Incorporated into the Virion in Significantly Smaller Amounts than Gag and Is Phosphorylated in Infected Cells." *Journal of Virology* 74 (20): 9727–31.

bioRxiv preprint doi: https://doi.org/10.1101/2021.09.14.460218; this version posted September 14, 2021. The copyright holder for this preprint (which was not certified by peer review) is the author/funder, who has granted bioRxiv a license to display the preprint in perpetuity. It is made available under aCC-BY 4.0 International license.

https://doi.org/10.1128/jvi.74.20.9727-9731.2000.

Müller, Thorsten G., Volkan Sakin, and Barbara Müller. 2019. "A Spotlight on Viruses—Application of Click Chemistry to Visualize Virus-Cell Interactions." *Molecules* 24 (3). https://doi.org/10.3390/molecules24030481.

Müller, Thorsten G., Vojtech Zila, Kyra Peters, Sandra Schifferdecker, Mia Stanic, Bojana Lucic, Vibor Laketa, Marina Lusic, Barbara Müller, and Hans Georg Kräusslich. 2021. "Hiv-1 Uncoating by Release of Viral Cdna from Capsid-like Structures in the Nucleus of Infected Cells." *ELife* 10: 1–32. https://doi.org/10.7554/ELIFE.64776.

Nikić, Ivana, Gemma Estrada Girona, Jun Hee Kang, Giulia Paci, Sofya Mikhaleva, Christine Koehler, Nataliia V. Shymanska, Camilla Ventura Santos, Daniel Spitz, and Edward A. Lemke. 2016. "Debugging Eukaryotic Genetic Code Expansion for Site-Specific Click-PAINT Super-Resolution Microscopy." *Angewandte Chemie - International Edition* 55 (52): 16172–76. https://doi.org/10.1002/anie.201608284.

Nikić, Ivana, and Edward A. Lemke. 2015. "Genetic Code Expansion Enabled Site-Specific Dual-Color Protein Labeling: Superresolution Microscopy and Beyond." *Current Opinion in Chemical Biology* 28: 164–73. https://doi.org/10.1016/j.cbpa.2015.07.021.

Novikova, Mariia, Yulan Zhang, Eric O. Freed, and Ke Peng. 2019. "Multiple Roles of HIV-1 Capsid during the Virus Replication Cycle." *Virologica Sinica* 34 (2): 119–34. https://doi.org/10.1007/s12250-019-00095-3.

Nunzio, Francesca Di, Thomas Fricke, Annarita Miccio, Jose Carlos Valle-Casuso, Patricio Perez, Philippe Souque, Ermanno Rizzi, et al. 2013. "Nup153 and Nup98 Bind the HIV-1 Core and Contribute to the Early Steps of HIV-1 Replication." *Virology* 440 (1): 8–18. https://doi.org/10.1016/j.virol.2013.02.008.

Paul-Gilloteaux, Perrine, Xavier Heiligenstein, Martin Belle, Marie Charlotte Domart, Banafshe Larijani, Lucy Collinson, Graça Raposo, and Jean Salamero. 2017. "EC-CLEM: Flexible Multidimensional Registration Software for Correlative Microscopies." *Nature Methods* 14 (2): 102–3. https://doi.org/10.1038/nmeth.4170.

Pear, W. S., G. P. Nolan, M. L. Scott, and D. Baltimore. 1993. "Production of High-Titer Helper-Free Retroviruses by Transient Transfection." *Proceedings of the National*

bioRxiv preprint doi: https://doi.org/10.1101/2021.09.14.460218; this version posted September 14, 2021. The copyright holder for this preprint (which was not certified by peer review) is the author/funder, who has granted bioRxiv a license to display the preprint in perpetuity. It is made available under aCC-BY 4.0 International license.

Academy of Sciences 90 (18): 8392–96. https://doi.org/10.1073/pnas.90.18.8392.

Pereira, Cândida F., Paula C. Ellenberg, Kate L. Jones, Tara L. Fernandez, Redmond P. Smyth, David J. Hawkes, Marcel Hijnen, et al. 2011. "Labeling of Multiple HIV-1 Proteins with the Biarsenical-Tetracysteine System." *PLoS ONE* 6 (2). https://doi.org/10.1371/journal.pone.0017016.

Permanyer, Marc, Ester Ballana, and José A. Esté. 2010. "Endocytosis of HIV: Anything Goes." *Trends in Microbiology* 18 (12): 543–51. https://doi.org/10.1016/j.tim.2010.09.003.

Pizzato, Massimo, Otto Erlwein, David Bonsall, Stephen Kaye, David Muir, and Myra O. McClure. 2009. "A One-Step SYBR Green I-Based Product-Enhanced Reverse Transcriptase Assay for the Quantitation of Retroviruses in Cell Culture Supernatants." *Journal of Virological Methods* 156 (1–2): 1–7. https://doi.org/10.1016/j.jviromet.2008.10.012.

Pornillos, Owen, Barbie K. Ganser-Pornillos, Sankaran Banumathi, Yuanzi Hua, and Mark Yeager. 2010. "Disulfide Bond Stabilization of the Hexameric Capsomer of Human Immunodeficiency Virus." *Journal of Molecular Biology* 401 (5): 985–95. https://doi.org/10.1016/j.jmb.2010.06.042.

Pornillos, Owen, Barbie K. Ganser-Pornillos, and Mark Yeager. 2011. "Atomic-Level Modelling of the HIV Capsid." *Nature* 469 (7330): 424–27. https://doi.org/10.1038/nature09640.

Price, Amanda J., Adam J. Fletcher, Torsten Schaller, Tom Elliott, Kyeong Eun Lee, Vineet N. KewalRamani, Jason W. Chin, Greg J. Towers, and Leo C. James. 2012. "CPSF6 Defines a Conserved Capsid Interface That Modulates HIV-1 Replication." *PLoS Pathogens* 8 (8). https://doi.org/10.1371/journal.ppat.1002896.

Price, Amanda J., David A. Jacques, William A. McEwan, Adam J. Fletcher, Sebastian Essig, Jason W. Chin, Upul D. Halambage, Christopher Aiken, and Leo C. James. 2014. "Host Cofactors and Pharmacologic Ligands Share an Essential Interface in HIV-1 Capsid That Is Lost upon Disassembly." *PLoS Pathogens* 10 (10). https://doi.org/10.1371/journal.ppat.1004459.

Rankovic, Sanela, Ruben Ramalho, Christopher Aiken, and Itay Rousso. 2018. "PF74 Reinforces the HIV-1 Capsid To Impair Reverse Transcription-Induced Uncoating." *Journal of Virology* 92 (20). https://doi.org/10.1128/jvi.00845-18.

bioRxiv preprint doi: https://doi.org/10.1101/2021.09.14.460218; this version posted September 14, 2021. The copyright holder for this preprint (which was not certified by peer review) is the author/funder, who has granted bioRxiv a license to display the preprint in perpetuity. It is made available under aCC-BY 4.0 International license.

Rasaiyaah, Jane, Choon Ping Tan, Adam J. Fletcher, Amanda J. Price, Caroline Blondeau, Laura Hilditch, David A. Jacques, et al. 2013. "HIV-1 Evades Innate Immune Recognition through Specific Cofactor Recruitment." *Nature* 503 (7476): 402–5. https://doi.org/10.1038/nature12769.

Rebensburg, Stephanie V., Guochao Wei, Ross C. Larue, Jared Lindenberger, Ashwanth C. Francis, Arun S. Annamalai, James Morrison, et al. 2021. "Sec24C Is an HIV-1 Host Dependency Factor Crucial for Virus Replication." *Nature Microbiology* 6 (4): 435–44. https://doi.org/10.1038/s41564-021-00868-1.

Rensen, Elena, Florian Mueller, Viviana Scoca, Jyotsana J Parmar, Philippe Souque, Christophe Zimmer, and Francesca Di Nunzio. 2021. "Clustering and Reverse Transcription of HIV-1 Genomes in Nuclear Niches of Macrophages." *The EMBO Journal* 40 (1): 1–16. https://doi.org/10.15252/embj.2020105247.

Rihn, Suzannah J., Sam J. Wilson, Nick J. Loman, Mudathir Alim, Saskia E. Bakker, David Bhella, Robert J. Gifford, Frazer J. Rixon, and Paul D. Bieniasz. 2013. "Extreme Genetic Fragility of the HIV-1 Capsid." *PLoS Pathogens* 9 (6). https://doi.org/10.1371/journal.ppat.1003461.

Rodriguez, Erik A., Henry A. Lester, and Dennis A. Dougherty. 2007. "Improved Amber and Opal Suppressor TRNAs for Incorporation of Unnatural Amino Acids in Vivo. Part 1: Minimizing Misacylation." *Rna* 13 (10): 1703–14. https://doi.org/10.1261/rna.666807.

Rubino, Frederick A., Yoon Hyeun Oum, Lakshmi Rajaram, Yanjie Chu, and Isaac S. Carrico. 2012. "Chemoselective Modification of Viral Surfaces via Bioorthogonal Click Chemistry." *Journal of Visualized Experiments*, no. 66: 1–7. https://doi.org/10.3791/4246.

Sakin, Volkan, Janina Hanne, Jessica Dunder, Maria Anders-Össwein, Vibor Laketa, Ivana Nikić, Hans Georg Kräusslich, Edward A. Lemke, and Barbara Müller. 2017. "A Versatile Tool for Live-Cell Imaging and Super-Resolution Nanoscopy Studies of HIV-1 Env Distribution and Mobility." *Cell Chemical Biology* 24 (5): 635-645.e5. https://doi.org/10.1016/j.chembiol.2017.04.007.

Sattentau, Quentin J. 2010. "Cell-to-Cell Spread of Retroviruses." *Viruses* 2 (6): 1306–21. https://doi.org/10.3390/v2061306.

Schaller, Torsten, Karen E. Ocwieja, Jane Rasaiyaah, Amanda J. Price, Troy L. Brady,

bioRxiv preprint doi: https://doi.org/10.1101/2021.09.14.460218; this version posted September 14, 2021. The copyright holder for this preprint (which was not certified by peer review) is the author/funder, who has granted bioRxiv a license to display the preprint in perpetuity. It is made available under aCC-BY 4.0 International license.

Shoshannah L. Roth, Stéphane Hué, et al. 2011. "HIV-1 Capsid-Cyclophilin Interactions Determine Nuclear Import Pathway, Integration Targeting and Replication Efficiency." *PLoS Pathogens* 7 (12). https://doi.org/10.1371/journal.ppat.1002439.

Schindelin, Johannes, Ignacio Arganda-Carreras, Erwin Frise, Verena Kaynig, Mark Longair, Tobias Pietzsch, Stephan Preibisch, et al. 2012. "Fiji: An Open-Source Platform for Biological-Image Analysis." *Nature Methods* 9 (7): 676–82. https://doi.org/10.1038/nmeth.2019.

Schmied, Wolfgang H., Simon J. Elsässer, Chayasith Uttamapinant, and Jason W. Chin. 2014. "Efficient Multisite Unnatural Amino Acid Incorporation in Mammalian Cells via Optimized Pyrrolysyl TRNA Synthetase/TRNA Expression and Engineered ERF1." *Journal of the American Chemical Society* 136 (44): 15577–83. https://doi.org/10.1021/ja5069728.

Schorb, Martin, Leander Gaechter, Ori Avinoam, Frank Sieckmann, Mairi Clarke, Cecilia Bebeacua, Yury S. Bykov, Andreas F.P. Sonnen, Reinhard Lihl, and John A.G. Briggs. 2017. "New Hardware and Workflows for Semi-Automated Correlative Cryo-Fluorescence and Cryo-Electron Microscopy/Tomography." *Journal of Structural Biology* 197 (2): 83–93. https://doi.org/10.1016/j.jsb.2016.06.020.

Schwedler, Uta K. von, Kirsten M. Stray, Jennifer E. Garrus, and Wesley I. Sundquist. 2003. "Functional Surfaces of the Human Immunodeficiency Virus Type 1 Capsid Protein." *Journal of Virology* 77 (9): 5439–50. https://doi.org/10.1128/jvi.77.9.5439-5450.2003.

Selyutina, Anastasia, Mirjana Persaud, Kyeongeun Lee, Vineet KewalRamani, and Felipe Diaz-Griffero. 2020. "Nuclear Import of the HIV-1 Core Precedes Reverse Transcription and Uncoating." *Cell Reports* 32 (13): 108201. https://doi.org/10.1016/j.celrep.2020.108201.

Seo, Jai Woong, Elizabeth S. Ingham, Lisa Mahakian, Spencer Tumbale, Bo Wu, Sadaf Aghevlian, Shahin Shams, et al. 2020. "Positron Emission Tomography Imaging of Novel AAV Capsids Maps Rapid Brain Accumulation." *Nature Communications* 11 (1): 1–13. https://doi.org/10.1038/s41467-020-15818-4.

Shi, J., J. Zhou, V. B. Shah, C. Aiken, and K. Whitby. 2011. "Small-Molecule Inhibition

bioRxiv preprint doi: https://doi.org/10.1101/2021.09.14.460218; this version posted September 14, 2021. The copyright holder for this preprint (which was not certified by peer review) is the author/funder, who has granted bioRxiv a license to display the preprint in perpetuity. It is made available under aCC-BY 4.0 International license.

of Human Immunodeficiency Virus Type 1 Infection by Virus Capsid Destabilization." *Journal of Virology* 85 (1): 542–49. https://doi.org/10.1128/jvi.01406-10.

Si, L., H. Xu, X. Zhou, Z. Zhang, Z. Tian, Y. Wang, Y. Wu, et al. 2020. "Erratum: Generation of Influenza A Viruses as Live but Replication-Incompetent Virus Vaccines (Science DOI: 10.1126/Science.Aah5869)." *Science* 369 (6508): 1–5. https://doi.org/10.1126/SCIENCE.ABE5323.

Smith, Stephen D., Margaret Shatsky, Pamela S. Cohen, Roger Wamke, Michael P. Link, and Bertil E. Glader. 1984. "Monoclonal Antibody and Enzymatic Profiles of Human Malignant T-Lymphoid Cells and Derived Cell Lines." *Cancer Research* 44 (December): 5657–60.

Strober, W. 2001. "Trypan Blue Exclusion Test of Cell Viability." *Current Protocols in Immunology / Edited by John E. Coligan ... [et Al.]* Appendix 3: 2–3. https://doi.org/10.1002/0471142735.ima03bs21.

Thadani, Nicole N., Christopher Dempsey, Julia Zhao, Sonya M. Vasquez, and Junghae Suh. 2018. "Reprogramming the Activatable Peptide Display Function of Adeno-Associated Virus Nanoparticles." *ACS Nano* 12 (2): 1445–54. https://doi.org/10.1021/acsnano.7b07804.

Thenin-Houssier, Suzie, and Susana T Valente. 2016. "HIV-1 Capsid Inhibitors as Antiretroviral Agents HHS Public Access." *Curr HIV Res* 14 (3): 270–82.

Toccafondi, Elenia, Daniela Lener, and Matteo Negroni. 2021. "HIV-1 Capsid Core: A Bullet to the Heart of the Target Cell." *Frontiers in Microbiology* 12 (April): 1–17. https://doi.org/10.3389/fmicb.2021.652486.

Uttamapinant, Chayasith, Jonathan D. Howe, Kathrin Lang, Václav Beránek, Lloyd Davis, Mohan Mahesh, Nicholas P. Barry, and Jason W. Chin. 2015. "Genetic Code Expansion Enables Live-Cell and Super-Resolution Imaging of Site-Specifically Labeled Cellular Proteins." *Journal of the American Chemical Society* 137 (14): 4602–5. https://doi.org/10.1021/ja512838z.

Wang, Nanxi, Yue Li, Wei Niu, Ming Sun, Ronald Cerny, Qingsheng Li, and Jiantao Guo. 2014. "Construction of a Live-Attenuated HIV-1 Vaccine through Genetic Code Expansion." *Angewandte Chemie International Edition* 53 (19): 4867–71. https://doi.org/10.1002/anie.201402092.

bioRxiv preprint doi: https://doi.org/10.1101/2021.09.14.460218; this version posted September 14, 2021. The copyright holder for this preprint (which was not certified by peer review) is the author/funder, who has granted bioRxiv a license to display the preprint in perpetuity. It is made available under aCC-BY 4.0 International license.

Waskom M, O Botvinnik, J Ostblom, S Lukauskas, P Hobson, DC Gemperline, T Augspurger, et al. 2020. "Constantine Evans, Version Mwaskom/Seaborn: V0.10.0." *Zenodo*. https://doi.org/https://doi.org/10.5281/zenodo.3629446.

Wei, Xiping, Julie M Decker, Hongmei Liu, Zee Zhang, Ramin B Arani, J Michael Kilby, Michael S Saag, Xiaoyun Wu, George M Shaw, and John C Kappes. 2002. "Emergence of Resistant Human Immunodeficiency Virus Type 1 in Patients Receiving Fusion Inhibitor (T-20) Monotherapy." *Antimicrob Agents Chemother* 46 (6): 1896–1905. https://doi.org/10.1128/AAC.46.6.1896.

Weigel, P. H., and J. A. Oka. 1981. "Temperature Dependence of Endocytosis Mediated by the Asialoglycoprotein Receptor in Isolated Rat Hepatocytes. Evidence for Two Potentially Rate-Limiting Steps." *Journal of Biological Chemistry* 256 (6): 2615–17. https://doi.org/10.1016/s0021-9258(19)69656-0.

Xu, Hongzhan, Tamera Franks, Gregory Gibson, Kelly Huber, Nadia Rahm, Caterina Strambio De Castillia, Jeremy Luban, et al. 2013. "Evidence for Biphasic Uncoating during HIV-1 Infection from a Novel Imaging Assay." *Retrovirology* 10 (1): 1–16. https://doi.org/10.1186/1742-4690-10-70.

Yang, Y., T. Fricke, and F. Diaz-Griffero. 2013. "Inhibition of Reverse Transcriptase Activity Increases Stability of the HIV-1 Core." *Journal of Virology* 87 (1): 683–87. https://doi.org/10.1128/jvi.01228-12.

Yang, Yang, Jeremy Luban, and Felipe Diaz-Griffero. 2014. "The Fate of HIV-1 Capsid: A Biochemical Assay for HIV-1 Uncoating." *Methods in Molecular Biology* 1087: 29–36. https://doi.org/10.1007/978-1-62703-670-2_3.

Yuan, Zhe, Nanxi Wang, Guobin Kang, Wei Niu, Qingsheng Li, and Jiantao Guo. 2017. "Controlling Multicycle Replication of Live-Attenuated HIV-1 Using an Unnatural Genetic Switch." *ACS Synthetic Biology* 6 (4): 721–31. https://doi.org/10.1021/acssynbio.6b00373.

Zhang, Chuanling, Xueying Zhou, Tianzhuo Yao, Zhenyu Tian, and Demin Zhou. 2018. "Precision Fluorescent Labeling of an Adeno-Associated Virus Vector to Monitor the Viral Infection Pathway." *Biotechnology Journal* 13 (4): 1–11. https://doi.org/10.1002/biot.201700374.

Zhao, Gongpu, Juan R. Perilla, Ernest L. Yufenyuy, Xin Meng, Bo Chen, Jiying Ning, Jinwoo Ahn, et al. 2013. "Mature HIV-1 Capsid Structure by Cryo-Electron

bioRxiv preprint doi: https://doi.org/10.1101/2021.09.14.460218; this version posted September 14, 2021. The copyright holder for this preprint (which was not certified by peer review) is the author/funder, who has granted bioRxiv a license to display the preprint in perpetuity. It is made available under aCC-BY 4.0 International license.

Microscopy and All-Atom Molecular Dynamics." *Nature* 497 (7451): 643–46. https://doi.org/10.1038/nature12162.

Zila, Vojtech, Erica Margiotta, Beata Turoňová, Thorsten G. Müller, Christian E. Zimmerli, Simone Mattei, Matteo Allegretti, et al. 2021. "Cone-Shaped HIV-1 Capsids Are Transported through Intact Nuclear Pores." *Cell* 184 (4): 1032-1046.e18. https://doi.org/10.1016/j.cell.2021.01.025.

Zila, Vojtech, Thorsten G. Müller, Vibor Laketa, Barbara Müller, and Hans-Georg Kräusslich. 2019. "Analysis of CA Content and CPSF6 Dependence of Early HIV-1" 10 (6): 1–20.

Zurnic Bönisch, Irena, Lieve Dirix, Veerle Lemmens, Doortje Borrenberghs, Flore De Wit, Frank Vernaillen, Susana Rocha, et al. 2020. "Capsid-Labelled HIV To Investigate the Role of Capsid during Nuclear Import and Integration." Edited by Frank Kirchhoff. *Journal of Virology* 94 (7): 1–29. https://doi.org/10.1128/JVI.01024-19.